ARMY RESEARCH LABORATORY

Effects of Machining on the Uniaxial and Equibiaxial Flexure Strength of CAP3 AD-995 Al_2O_3

by Andrew A. Wereszczak, Jeffrey J. Swab, and Reuben H. Kraft

ARL-TR-3617 **September 2005**

NOTICES

Disclaimers

The findings in this report are not to be construed as an official Department of the Army position unless so designated by other authorized documents.

Citation of manufacturer's or trade names does not constitute an official endorsement or approval of the use thereof.

Destroy this report when it is no longer needed. Do not return it to the originator.

Army Research Laboratory
Aberdeen Proving Ground, MD 21005-5069

ARL-TR-3617 **September 2005**

Effects of Machining on the Uniaxial and Equibiaxial Flexure Strength of CAP3 AD-995 Al_2O_3

Andrew A. Wereszczak, Jeffrey J. Swab, and Reuben H. Kraft
Weapons and Materials Research Directorate, ARL

REPORT DOCUMENTATION PAGE	Form Approved OMB No. 0704-0188

1. REPORT DATE *(DD-MM-YYYY)*	2. REPORT TYPE	3. DATES COVERED (From - To)
September 2005	Final	March 2001–February 2002

4. TITLE AND SUBTITLE
Effects of Machining on the Uniaxial and Equibiaxial Flexure Strength of CAP3 AD-995 Al_2O_3

5a. CONTRACT NUMBER

5b. GRANT NUMBER

5c. PROGRAM ELEMENT NUMBER

6. AUTHOR(S)
Andrew A. Wereszczak, Jeffrey J. Swab, and Reuben H. Kraft

5d. PROJECT NUMBER
622105H84

5e. TASK NUMBER

5f. WORK UNIT NUMBER

7. PERFORMING ORGANIZATION NAME(S) AND ADDRESS(ES)
U.S. Army Research Laboratory
ATTN: AMSRD-ARL-WM-MB
Aberdeen Proving Ground, MD 21005-5069

8. PERFORMING ORGANIZATION REPORT NUMBER
ARL-TR-3617

9. SPONSORING/MONITORING AGENCY NAME(S) AND ADDRESS(ES)

10. SPONSOR/MONITOR'S ACRONYM(S)

11. SPONSOR/MONITOR'S REPORT NUMBER(S)

12. DISTRIBUTION/AVAILABILITY STATEMENT
Approved for public release; distribution is unlimited.

13. SUPPLEMENTARY NOTES

14. ABSTRACT
The effect of surface condition on the uniaxial and equibiaxial flexure strength of CoorsTek's CAP3 AD-995 alumina was examined. (Note that this material was found not to be the same as CoorsTek's AD-955 alumina—a comparison and discussion of the differences are provided in this report.) The following four surface conditions were considered: as-fired (i.e., unmachined) surfaces; the condition produced by CoorsTek's standard surface-grinding procedures (i.e., the condition they will provide on tiles unless otherwise specified); the condition resulting from uniaxial surface grinding with 320-grit diamond machining (i.e., that surface machining method specified for ASTM C1161-94 ceramic flexure bars); and rotary surface grinding with 320-grit diamond machining. Equibiaxial flexure strengths were ~20% less than uniaxial flexure strengths for all of the four investigated surface conditions. This amount correlates very well with predicted strength-size scaling between the two geometries using the Weibull theory. Because this failure stress is lower, and probably more representative of on-center ballistic loading of ceramic tiles, its use is conservative and perhaps better suited as input for ballistic models that consider such deflections. The results from this study show that machining practices can be employed to increase flexure strength which may have beneficial ramifications on ballistic performance. Issues of flexure-strength dependence on surface conditioning are likely to be more relevant under certain combinations of the tile thickness and impact load. Similar testing should be conducted on the stronger, finer-grained SiC armor ceramics, since the affect of machining on flexure strength may be more pronounced.

15. SUBJECT TERMS
alumina, flexure strength, armor ceramics, machining, microstructure

16. SECURITY CLASSIFICATION OF:			17. LIMITATION OF ABSTRACT	18. NUMBER OF PAGES	19a. NAME OF RESPONSIBLE PERSON
a. REPORT	b. ABSTRACT	c. THIS PAGE			Andrew A. Wereszczak
UNCLASSIFIED	UNCLASSIFIED	UNCLASSIFIED	UL	70	19b. TELEPHONE NUMBER (*Include area code*) 410-306-0753

Standard Form 298 (Rev. 8/98)
Prescribed by ANSI Std. Z39.18

Contents

List of Figures

List of Tables

Acknowledgments

This research was supported in part by an appointment to the Research Participation Program at the U.S. Army Research Laboratory (ARL) administered by the Oak Ridge Institute for Science and Education through an interagency agreement between the U.S. Department of Energy and ARL.

Gratitude is expressed for some of the SEM imaging performed by ORNL's H. T. Lin, the coordination of the fixturing machining performed by ORNL's J. E. Shelton and M. K. Ferber, and the piezoluminescence characterization performed by ORNL's M. J. Lance. The authors also wish to thank NIST's G. D. Quinn for his comments and input. Lastly, C. Hoppel, S. Ghiorse, S. McSpadden, and M. Radovic are thanked for reviewing the manuscript and for their useful comments.

INTENTIONALLY LEFT BLANK.

Executive Summary

The effect of surface condition on the uniaxial and equibiaxial flexure strength of CoorsTek's CAP3 AD-995 alumina was examined. Note that this material was found *not* to be the same as CoorsTek's AD-995 alumina—a comparison and discussion of their differences are provided in this report. The following four surface conditions were considered with the CAP3 AD-995: as-fired (i.e., unmachined) surfaces; the condition produced by CoorsTek's standard surface grinding procedures (i.e., the condition they will provide on tiles unless otherwise specified); the condition resulting from uniaxial surface grinding with 320-grit diamond machining (i.e., that surface machining method specified for ASTM C1161-94 ceramic flexure bars); and rotary surface grinding with 320-grit diamond machining.

CoorsTek manufactures and markets two grades of compositionally equivalent, 99.5%-purity alumina, designated by CoorsTek as AD-995 and CAP3 AD-995; the latter was tested in the present study. Unfortunately, confusion often results when examining the literature because of that compositional equivalency and because authors often tend to generically report both as AD-995, so it is difficult (if not impossible) for readers to discern which of the two CoorsTek 99.5% alumina grades was interrogated unless microstructural evaluations were actually performed and reported. Adding to this confusion is the fact that CoorsTek reports the same average grain size (and other properties too) for these two 99.5% grades (though an average size of 1.5 and 5.7 μm was respectively measured for AD-995 and CAP3 AD-995 in the present study); though their values may be statistically correct, the narrow and wide grain size distributions of the AD-995 and CAP3 AD-995 grades respectively are not illustrated by that mean value. Microstructures for both grades are reported and described to show the differences and to promote to future investigators of either grade of AD-995 that it behooves them to understand the microstructure of the AD-995 and to recognize which of the two grades that they are actually investigating. The understanding of their differences is important, as the AD-995 alumina is omnipresent in the structural ceramic literature whereas CAP3 AD-995 is somewhat relegated to the armor community (though suspicion exists that AD-995 is actually the 99.5% alumina grade that is often ballistically- or high-strain-rate tested—that suspicion unfortunately cannot be supported nor denied unless grain size distribution information or microstructures accompanied those studies).

Uniaxial flexure strength testing was performed because it is the most common and recognizable strength test for ceramics, and equibiaxial* flexure strength testing was conducted because it is believed to better mimic (than uniaxial flexure testing) the deflection that results from on-center

*There are many types of "biaxial" strength tests. An "equi"-biaxial strength test is a special case of general "biaxial" strength testing where the two principal stresses have the same sign and magnitude in the specimen gage section.

ballistic loading of armor tiles. Interest existed to link the generated strength distributions from the two flexure test configurations while examining how surface condition affected both.

Both flexure tests utilized established and demonstrated practices. Uniaxial flexure strength testing adhered to ASTM C1161 practices and involved four-point bending of "B"-size bars sectioned from tiles that had one of the four surface conditions; that surface condition was oriented to be on the tensile face of the bend specimen. The effect of chamfered (or unchamfered) bend bar edges on uniaxial flexure strength was also examined. Equibiaxial flexure strength testing consisted of concentric ring-on-ring testing of tiles in which the surface condition was oriented to be on the tensile face of the tile specimen. The surface area sampled by the equibiaxial flexure testing was more than one order of magnitude larger than that sampled by the uniaxial flexure testing.

Not surprisingly, strength depended on surface condition. Surfaces that were uniaxial or rotary ground using 320-grit diamond machining generated the highest strengths (equibiaxial flexure characteristic strength = 280 MPa), followed in descending order of strengths from as-fired surfaces (equibiaxial flexure characteristic strength = 264 MPa), and then strengths from surfaces produced by CoorsTek's standard grinding procedure (equibiaxial flexure characteristic strength = 244 MPa). Those differences in strengths are statistically significant with 95% confidence. These results show that finer surface finishes produced by 320-grit machining can increase flexure strength, and suggest that CoorsTek's standard surface grinding procedure of CAP3 AD-995 tiles is perhaps too aggressive.

The balancing of the extra cost of machining CAP3 AD-995 alumina and its beneficial effect on strength needs to proceed with caution. First, though CoorsTek's "standard" machining will provide a tile whose dimensions will have stricter tolerances than those of "as-fired" tiles for an extra cost of $14/tile (tile geometry = 4 × 4 × 0.118 in), that comes at the expense of lower strengths—a 7–8% decrease. The strength of 320-grit machined tiles was 6% and 15% greater than tiles with as-fired surfaces and CoorsTek "standard" ground surfaces, respectively, but that resulted from an additional machining expense of $45/tile. If desire remains to have CoorsTek perform the surface machining of their CAP3-AD995 alumina tiles, then a requested combination of a less aggressive machining practice and a finer-grit grinding wheel should be considered by the customer. Clearly, the 320-grit machining benefits strength; however, the justification of the extra expense for that relatively low amount of strengthening is subjective and will depend on the needs of the end-user.

As expected, chamfering edges on specimens has a beneficial effect on uniaxial flexure strength. *Not* chamfering uniaxial flexure specimens resulted in a strength loss of approximately 4–8% for a given machining condition for CAP3 AD-995 alumina. The reduction in strength correlated with failure consistently being initiated at the edge of these specimens (an occurrence not observed when bend bar edges were chamfered). A lack of edge chamfering inherently has no effect on equibiaxial flexure strength; however, its presence may indeed be influential as a tile is

mechanically loaded closer to one of its edges (and that edge is chamfered versus unchamfered). Chamfering edges in ceramic specimens and components has been long recognized to increase strength; however, in spite of that recognized effect, the study of chamfered or unchamfered edges in the present study was revisited because ceramic tiles are still supplied by vendors with unchamfered edges and interest therefore existed to statistically illustrate their detrimental effect on strength.

Uniaxial flexure testing according to ASTM C1161 produced strengths that were dependent on the machining direction. The directional-dependence on uniaxial flexure strength was a consequence of the interaction between the extent of anistropic machining damage and the relatively large average grain size of CAP3 AD-995 alumina. The directional-dependence on uniaxial flexure strength effect only complicates the general interpretation of flexure strength dependence on surface condition, whereas equibiaxial flexure testing facilitates surface condition comparisons because of its "averaging effect" on machining directionality—it is perhaps a better flexure test for assessing flexure strength of armor tiles.

Equibiaxial flexure strengths were ~20% less than uniaxial flexure strengths for any of the four investigated surface conditions: this amount correlates well with predicted strength-size scaling between the two geometries using the Weibull theory. Because this failure stress is lower, and probably more representative of on-center ballistic loading of ceramic tiles, its use is conservative and perhaps better suited than the use of uniaxial flexure strength for input in ballistic models that consider such deflections.

The results from this study show that machining practices can be employed to increase flexure strength which may have beneficial ramifications on ballistic performance when thin tile are used. Issues of flexure strength dependence on surface condition are likely to be more relevant as armor tile thicknesses decrease. Bending-induced deflections for a given load (or impact) will increase as tile thickness decreases, and if those deflections are sufficient to cause (tensile stress induced) failure in the ceramic tile, then proactively increasing flexure strength (e.g., performing finer grit diamond machining) in the ceramic tile will lessen the likelihood of its failure for the same load or impact. Ceramic armor thicknesses that tend to be relatively thin (e.g., WC tiles, body armor) will likely be more affected by the surface finish than ceramic armor that is relatively thick (e.g., thick ceramic tiles in vehicular armor).

Conceivably, the equibiaxial flexure test apparatus and method utilized in the present study may be extended for use as a quality control "proof test" and discriminate stronger tiles from weaker ones. If stronger tiles (i.e., tiles that can withstand greater center-line deflection prior to fracturing) could be linked to better ballistic performance, then this equibiaxial flexure test could be used to filter out and eliminate from consideration those tiles that have low potential for poor ballistic performance.

INTENTIONALLY LEFT BLANK.

1. Introduction

There are several convoluted processes of ballistic impact in ceramic tiles that are often complicated to deconvolute and interpret. However, there are some aspects of the impact event that appear to have links to more established interpretations associated with the fracture event in "static" mechanical tests. For example, the fracture pattern in ceramic armor tiles that are on-center ballistically tested often has similarity to that resulting in ceramic specimens that fractured in "static" equibiaxial flexure strength testing. This observation is reasonable when the whole ballistic event is considered as a sum of localized projectile/tile interaction and macro-structural response of the ceramic tile to mechanical loading.

Ceramic "bend-strength" data is often used in ballistic models to predict performance of the ceramic tiles. Unfortunately, in this instance, the "bend-strength" of ceramics is an enigmatic parameter at best and non-conservative or misleading at worst. It has long been recognized that the (tensile) strength of monolithic ceramics exhibits "strength-size scaling" (i.e., "weakest-link-in-a-chain" analog). A large, ceramic specimen will fail at a lower stress than a smaller specimen of the same material. Strengths of ceramics typically are better represented by a Weibull distribution than a Gaussian distribution, and their relatively wide scatter has resulted in a combined, size-scaling, Weibull function that relates probability of failure to specimen size and applied stress (and stress gradient too). Further complicating this is the fact that the strength of ceramics, when loaded in flexure or when there is a tensile stress on their surface, is susceptible to the nature of surface condition (and, of course, how much surface area is under tension). Analogous to scratched or scored glass loaded in flexure, ceramics that have been coarsely machined will typically break at lower bend stresses than the same ceramic that was finely machined. Additionally, a coarse or aggressive machining step prior to finish grinding can introduce significant sub-surface damage that will tend to reduce strength—this can be particularly frustrating because the fine surface finish suggests to the end user that the strength should be relatively high, however, the hidden effects of the coarse machining often still dominate and reduce strength—an effect that is typically not observed until strength tests are performed, or worse yet, when the tile is unpredictably found not to be able to withstand appreciable bending in service. Introducing machining direction as an independent parameter also affects strength (i.e., the uniaxial flexure strength of a ceramic that was machined in the same direction as the applied tensile stress will typically be higher than when the machining direction is perpendicular to the applied tensile stress … for the same extent of machining damage). Because of these complications and trends, the use of a reported "bend strength" of a ceramic without knowing how the associated test specimens were prepared or mechanically tested is introducing danger, and is a primary reason why ASTM C1161-94 at (*1*) was developed to guide those evaluating the "bend strength" of ceramics.

There were several goals sought in the present study. The primary goal was to examine and portray the above-described static "bend strength" issues in a common armor ceramic, CoorsTek's CAP3 AD-995 alumina, so to make their effects of interest, relevance, and use to those in ballistic community. A second goal was to assess if and how alternative machining practices would affect the flexure strength of this alumina (with a hypothesis that a higher flexure strength can manifest itself in improved ballistic performance). Four surface conditions were considered as an independent parameter: as-fired (i.e., unmachined); the condition produced by CoorsTek's standard surface grinding procedures (i.e., the condition they will produce on tiles unless otherwise specified by the customer); the condition resulting from uniaxial surface grinding with 320-grit diamond machining (i.e., that surface machining method specified for ASTM C1161-94 ceramic flexure bars), and rotary surface grinding with 320-grit diamond machining. A third goal was to examine these surface conditions and strength-size scaling effects using two types of flexure tests: uniaxial and equibiaxial flexure.

Uniaxial flexure strength testing was performed because it is the most common and recognizable strength test for ceramics, and equibiaxial flexure strength testing was conducted because it samples a much larger surface and volume and because it is believed to better mimic (than uniaxial flexure testing) the deflection that results from on-center ballistic loading of armor tiles. Interest also existed in linking the strength distributions from the two flexure testing configurations while examining how surface condition affected both.

This report first describes the CAP3 AD-995 alumina, the employed mechanical tests and data analysis, and the independent parameters that were explored. Uniaxial and equibiaxial strengths are then reported, linked, and examined as a function of the investigated surface conditions. Lastly, their interpretations are described and suggested ramifications on ballistic performance are presented.

2. Experimental Procedures

A description of the CAP3 AD-995 alumina is presented first, followed by descriptions of the investigated surface conditions, the utilized flexure testing, and the data and fracture analyses.

2.1 CAP3 AD-995 Al_2O_3 Description

The class of an alumina per Mil Spec MIL-P-46199 (MR) (*2*) is associated with its purity. CAP3-AD995 alumina (Al_2O_3) is a Class 4 alumina, whereas the AD-85, AD-94, and AD-995 aluminas listed in table 1 are class 1, class 3, and class 4, respectively.

CoorsTek reports (*3*–*4*) the properties for CAP3 AD-995 alumina that are listed in table 1, and they are compared against other aluminas they manufacture. Note that CoorsTek reports the exact same property values for their "AD-995" and "CAP3 AD-995" grades; this suggests that

Table 1. Room temperature properties for a variety of CoorsTek aluminas as reported by CoorsTek (*3–4*). CAP3 AD-995 alumina was tested in the present study.

Property	Test	AD-85	AD-94	AD-995	CAP3 AD-995	AD-999
Purity (%)	—	85	94	99.5	99.5	99.9
Density (g/cm^3)	ASTM C20	3.42	3.70	3.90	3.90	3.96
Average grain (μm)	—	6	12	6	6	3
Flexure strength (MPa)	ASTM F417	296	352	379	379	552
Elastic modulus (GPa)	ASTM C848	221	303	370	370	386
Poisson's ratio	ASTM C848	0.22	0.21	0.22	0.22	0.22
Hardness (GPa)	Knoop 1000 g	9.4	11.5	14.1	14.1	15.2
Fracture toughness (MPa√m)	Notched beam	3–4	4–5	4–5	4–5	4–5

they intend the two compositions to be the same (our results will show that is not the case on their microstructures).

2.2 Machining Conditions

The investigated surface conditions that compromised the independent parameters of this study are described and listed in table 2 along with qualitative descriptions of the machining procedures that produced them. Tiles with nominal dimensions of 4 × 4 × 0.118 in (all ±1%) were purchased from CoorsTek. A fraction of them had "as-fired" surfaces while the remainder had "as-received" ground surfaces that were machined by CoorsTek per their "standard" grinding method. Their "standard" grinding method (*5*) consists of 80-grit diamond machining and involves rotary surface grinding. This "standard grinding" is the machining practice employed by CoorsTek on all armor tiles unless a surface finish requirement is specified. It was recognized that many such tiles are purchased having only dimensional tolerance requirements; consequently, it was of interest to characterize strength effect on this "standard" grinding method. The received tile length and width tolerances were within those (±2.0% or ±1.5 mm, whichever is greater) specified per MIL-P-46199 (MR) (*2*). Thickness tolerances were within those (±3.0% or ±0.5 mm, whichever is greater) allowable MIL-P-46199 (MR) too.

Many of the "as-received" tiles were further machined by a commercial ceramic machining company (Bomas Machine Specialties, Inc., Somerville, MA) with 320-grit diamond machining either using uniaxial or rotary surface grinding. The uniaxial grinding procedure (see figure 1) is recommended for machining uniaxial flexure specimens in

ASTM C1161-94 (*1*).* Rotary surface grinding (see figure 2) using the same 320-grit machining was of interest to see if a non-uniaxial surface grinding procedure yielded equivalent flexure strengths, and because ceramic vendors sometimes prefer to use that method over uniaxial surface grinding.

Table 2. The effects of five surface conditions on strength were investigated. Comparison of cost per tile (nominal dimensions: 4 × 4 × 0.118 in) shown.

Type of Surface or Descriptor	Description	Cost Per Tile
As-fired	Unadulterated surface resulting from sintering of tiles.	$33
As-received	CoorsTek "standard" grinding method that is used if a customer does not specify a surface finish. It is an 80-diamond-grit rotary grinding process (*6*). CoorsTek offers 100-grit grinding for an additional 10% cost, but that was not pursued.	$42
Longitudinal[a]	Uniaxial surface grinding with a 320-diamond-grit wheel per ASTM C1161-94 (*1*). Grinding direction is oriented parallel with the major axis of the bend bar. Such directionality is not exploited by the ring-on-ring equibiaxial flexure testing.	$87 The 320-grit uniaxial surface grinding ($45) was performed on "as-received" tiles ($42). $87 is their sum.
Transverse[a]	Uniaxial surface grinding with a 320-diamond-grit wheel per ASTM C1161-94 (*1*). Grinding direction is oriented perpendicular with the major axis of the bend bar. Such directionality is not exploited by the ring-on-ring equibiaxial flexure testing.	$87 The 320-grit uniaxial surface grinding ($45) was performed on "as-received" tiles ($42). $87 is their sum.
Rotary ground[a]	Rotary surface grinding with a 320-diamond-grit wheel.	$87 The 320-grit rotary surface grinding ($45) was performed on "as-received" tiles ($42). $87 is their sum.

[a]Surfaces ground at Bomas Machine Specialties, Inc., Somerville, MA.

The final cost per tile for this specific geometry (in 2002 dollars) were as follows: $33 per tile for as-fired tiles; $42 per tile for as-received or CoorsTek-machined tiles; and $87 per tile for 320-grit uniaxial or rotary surface ground tiles.

*ASTM C1161-2002 is now a successor to ASTM C1161-1994, and it advocates progressive machining steps during grinding with a 400-600 grit wheel used in the final step. The 2002 version was not yet announced at the time the tiles in this study were machined, so the 320-grit finish machining advocated in the 1994 version was employed.

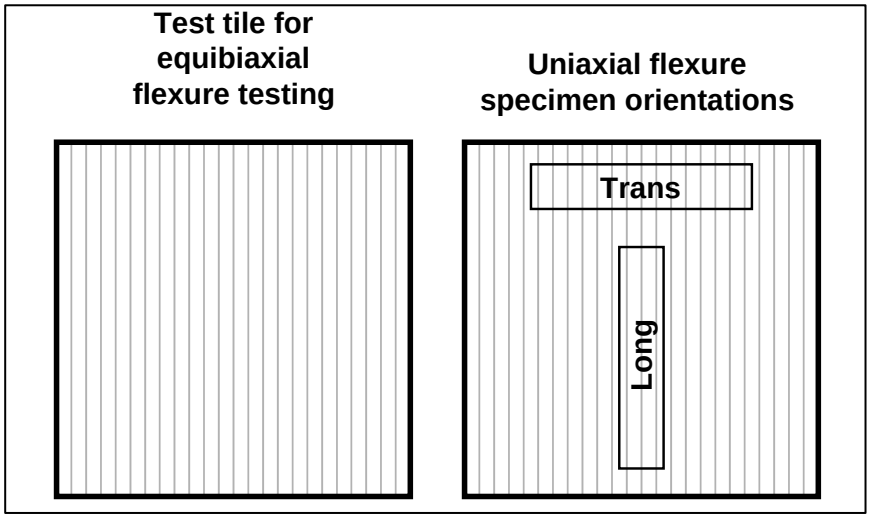

Figure 1. Schematic of grinding mark orientation on uniaxially ground tiles and how transversely and longitudinally machined bend bars were sectioned from them.

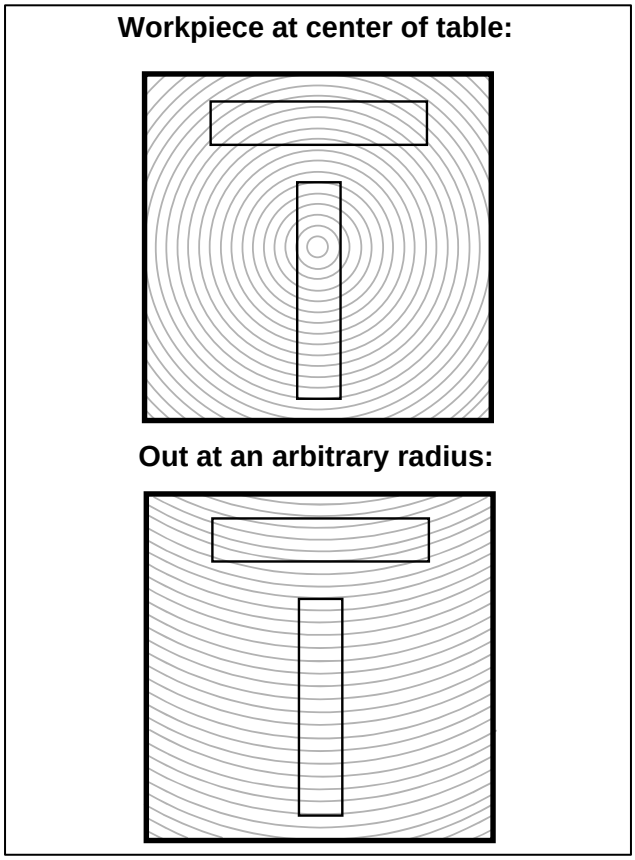

Figure 2. Schematic of grinding mark orientation on rotary ground tiles. Unfortunately, the location (radius) of the tile on the table of the rotary grinder and the orientation of how the bend bars were machined from the tiles were not monitored.

Uniaxial flexure specimens were sectioned out of the uniaxial and rotary surface ground tiles in the manner illustrated in figures 1 and 2. The sectioning of the tiles shows how directionality of machining is oriented with the primary length of the specimen, and portrays the differences in longitudinal and transverse grinding that are listed in table 2. The tracking and orientation of sectioned uniaxial flexure specimens out of rotary surface grind tiles was not documented. This was unfortunate because the grinding marks on such tiles are a function of the radial tile placement on the work table during machining; however, its effect (if any) on strength was not identified upon examination of equibiaxial flexure strengths.

2.3 Flexure Strength Testing

Uniaxial and equibiaxial flexure strength tests were performed using established and demonstrated practices. The surface area sampled by the equibiaxial flexure testing was more than one order of magnitude larger than that sampled by the uniaxial flexure testing, and this exploited the effect of strength-size scaling in this ceramic.

2.3.1 Uniaxial (ASTM C1161)

Uniaxial flexure strength testing adhered to ASTM C1161 practices (*1*) and involved four-point bending of type "B" bars sectioned from tiles that had one of the four surface conditions. One of those conditions, uniaxial surface grinding, was further examined by sectioning specimens both parallel (i.e., longitudinally ground) and perpendicular (i.e., transversely ground) to the direction of uniaxial grinding, so a total of five surface condition sets were examined with uniaxial flexure specimens. A minimum of 27 specimens were tested per surface condition outlined in table 2. Each of the five surface condition sets were examined by orienting their surface to be on the tensile face of the bend specimen and then tested in uniaxial flexure. A side-view schematic of the four-point-bend specimen and fixture is shown in figure 3. The specimen dimension was nominally 3 × 4 × 50 mm, and it was tested using a fixture having 20- and 40-mm upper and lower spans, respectively. The specimen was monotonically loaded to fracture using a displacement rate of 0.5 mm/min. The failure load (P) was used to calculate the uniaxial flexure strength (S_{1161B}) using

$$S_{1161B} = \frac{3P(L_L - L_U)}{2bh^2} \quad , \tag{1}$$

where L_L is the lower span (40 mm), L_U is the upper span (20 mm), b is the specimen base (4 mm), and h is the specimen thickness or height (3 mm).

The effect of chamfered (or unchamfered) bend bar edges on uniaxial flexure strength was also examined. Unchamferred bars from tiles that had as-fired, as-received, and rotary surface ground surfaces were considered. The motivation behind this was to quantify the recognized beneficial effect of edge-chamfering ceramic specimens (and ceramic components too, when allowed).

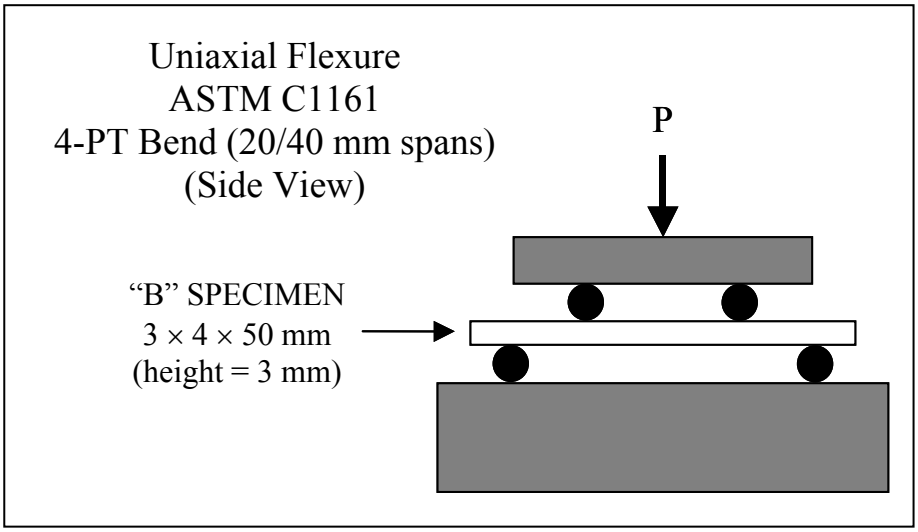

Figure 3. Side-view schematic of the uniaxial flexure strength test.

2.3.2 Equibiaxial

Equibiaxial flexure strength testing consisted of concentric ring-on-ring testing of tiles in which the surface condition was oriented to be on the tensile face during equibiaxial flexure.

2.3.2.1 Promoting Valid Equibiaxial Flexure Testing. Much consideration was devoted toward the design of the equibiaxial (concentric ring-on-ring or ROR) flexure fixture, and that was based on prior studies involving this test (*6–8*). The ROR configuration is preferred over the piston-on-three ball (PO3B) equibiaxial flexure test (such as ASTM F394 [*9*]) since it subjects a greater portion of the specimen to an equibiaxial stress state and it distributes the total applied contact load over a larger area of the specimen. This acts to reduce the applied stress concentration at the contact locations between the fixture and specimen which subsequently minimizes the likelihood of fixture-induced specimen failure (invalid test data). Cimpoeru (*10*) performed a ball-on-elastic-foundation study on 99%-purity alumina tiles; though failure load increase was observed with increasing tile thickness as expected, unfortunately no fractography was reported to substantiate that the stress concentration associated with the ball-loading did not cause the fracture events.

Even though the ROR configuration is more advantageous than the PO3B (*11*), care must still be taken to appropriately determine the diameters of the ROR configuration (relative to the specimen thickness) in order to promote a valid and linear elastic event. For example, if the ratio of the upper-ring diameter to the lower-ring diameter (D_U/D_L) is too low, then excessive deflection of the specimen can exist at the moment of fracture and result in error being introduced into the calculation of equibiaxial flexure strength due to nonlinear membrane-like stresses and even friction effects. Figures 4 and 5 illustrate the affect of a D_U/D_L that is too small. Conversely, if D_U/D_L is too high, then contact-stress-concentrations will increase and

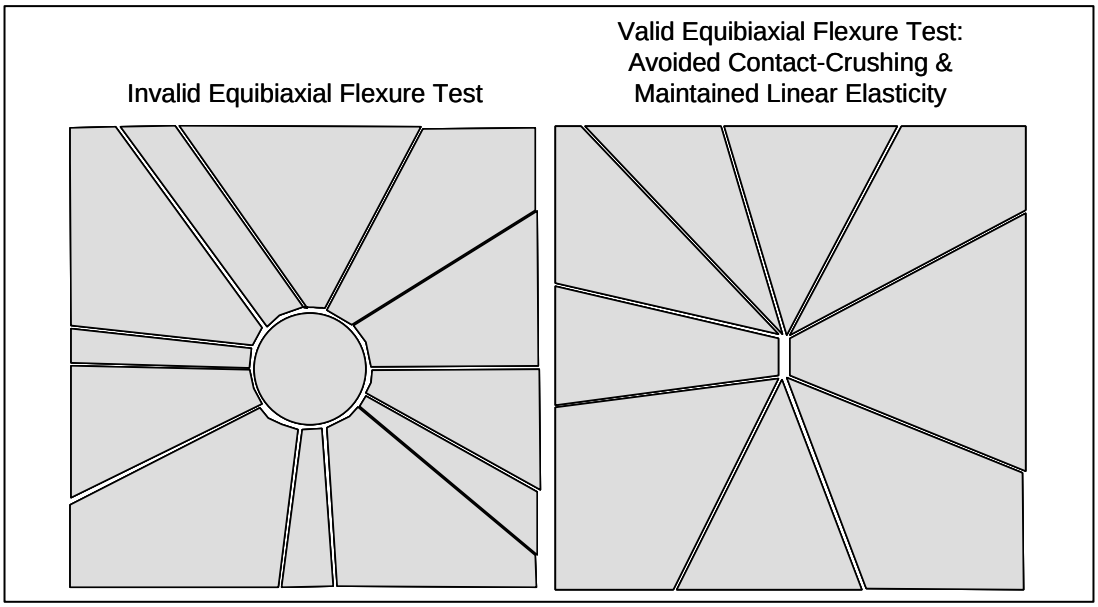

Figure 4. Appropriate determination of the diameters of the ring-pairs with respect to the specimen elastic properties and thickness will generate a valid equibiaxial flexure strength test. Schematic on the left shows an invalid test (upper ring "punching" a disk through a too-thin specimen). Schematic on the right shows a valid test (the two opposed pieces each having a flat contain the strength-limiting flaw).

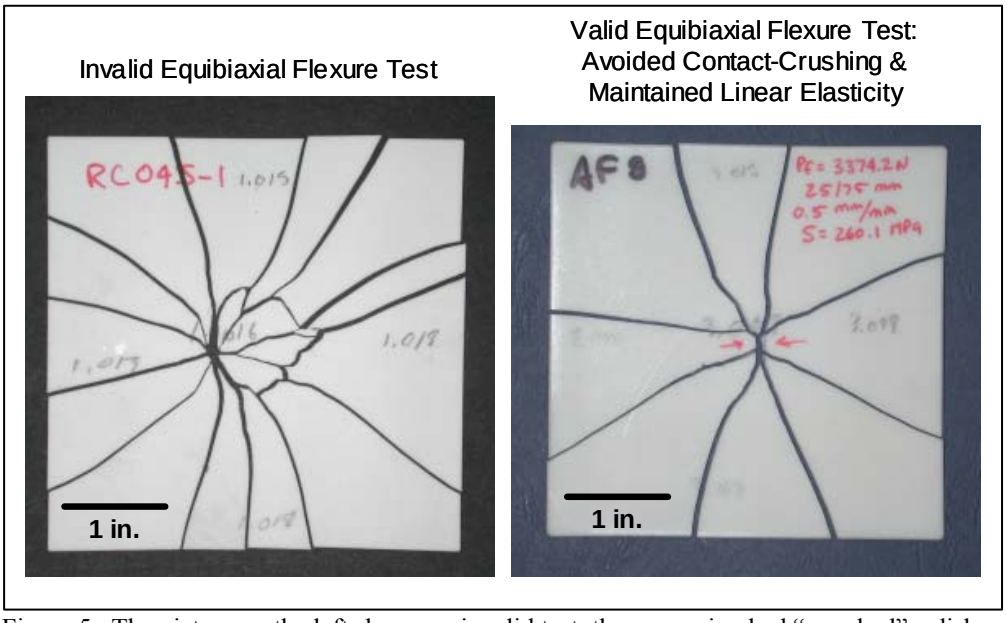

Figure 5. The picture on the left shows an invalid test; the upper ring had "punched" a disk of fragments through the too-thin specimen that had excessively deflected (i.e., the fixture had caused the fracture event). The picture on the right shows a valid test (i.e., the fixture did not cause the fracture event), and two arrows point to the mating fracture surface where the fracture event was initiated.

localized contact-crushing can occur resulting in an invalid fracture strength. The objective is to determine the range of D_U/D_L where linear elasticity is still valid and contact stresses are minimized; this is accomplished through the appropriate use of classical beam bending (strive to keep maximum deflection below 1/2 of the specimen thickness) and consideration of the materials elastic properties and specimen thickness. When that objective is met, then the test fixture will likely not cause fracture, the intrinsic specimen strength will be measured, and the fracture patterns in figures 4 and 5 are typically observed. The ASTM standard, ASTM C1499 (*12*), for equibiaxial flexure testing follows this rationale. Fracture patterns in figures 4 and 5 are not unlike fracture patterns that are sometimes observed in on-center ballistically evaluated ceramic tiles. Though this commonality is not further explored in this study, it is an important one nonetheless, and provides a glimpse of a possible link between the nature of fracture in equibiaxial flexure testing and that which occurs as a consequence of on-center impact ballistic loading of ceramic tiles.

2.3.2.2 Description of Fixturing. For the present study, the nominal tile thickness of the equibiaxial flexure specimen was 3 mm (0.118 in) and the elastic modulus of the CAP3 AD-995 alumina was ~370 GPa. Using principals described in section 2.3.2.1 resulted in a choice of a 25-mm diameter for the upper ring and a 75-mm diameter for the lower ring. A schematic of the assembled fixture is shown in figure 6 while dimensions, tolerances, and additional detail of the upper and lower rings are included in figures 7 and 8.

2.3.2.3 Test Procedure. Each tile was inserted in the fixture shown in figure 6 and then set in the load frame of an eletromechanical universal test machine. A steel sphere was positioned between the load cell and the top of the assembled equibiaxial flexure fixture to promote articulated loading (i.e., passive alignment). A displacement rate of 0.5 mm/min was used to load the specimen to fracture.

The equibiaxial flexure strength (S_{ROR}) was calculated using the fracture load (P) and the fixture and tile dimensions according to the following relationship (*13*, *14*):

$$S_{ROR} = \frac{3P}{4t^2\nu}\left[2(1+\nu)\ln\frac{D_L}{D_U} + \frac{(1-\nu)(D_L^{\,2} - D_U^{\,2})}{1.2L^2}\right], \qquad (2)$$

where t is the tile thickness (~3 mm), ν is Poisson's ratio, D_L is the diameter of the supporting or lower ring (75 mm), D_U is the diameter of the loading or upper ring (25 mm), and L is the tile edge length (~100 mm).

A minimum of six tiles were tested for each of the four grinding conditions. It would have been desirable to have tested a greater number of tiles per condition; however, the statistical analysis took into account these relatively low number of tests in the confidence bound estimations, so strength comparisons still had statistically significant results.

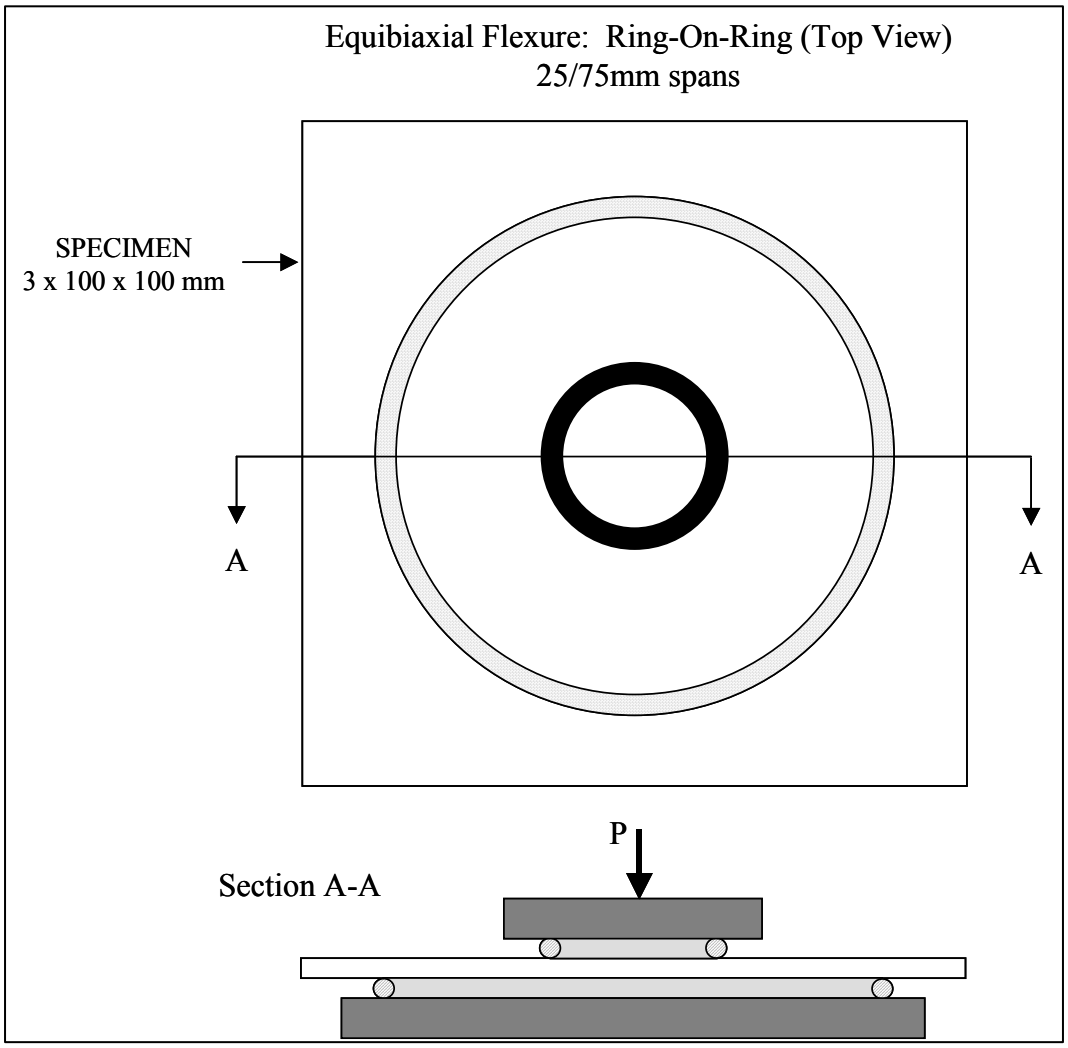

Figure 6. Top- and sectioned-view schematics of the equibiaxial flexure strength test.

2.4 Data and Fracture Analyses

The strength data was analyzed using a two-parameter Weibull distribution, and a description of that application follows. Fractography was performed to identify the type of strength-limiting flaw (as a function of surface condition) in both uniaxial and equibiaxially tested specimens, and a brief description of that effort is presented. Lastly, because the effective areas of the uniaxial and equibiaxial flexure specimens were quite different, a brief description of strength-size scaling issues in monolithic ceramics is presented.

2.4.1 Two-Parameter Weibull Distribution

The probability of failure (P_f) as a function of failure stress (S) is represented using the uncensored, two-parameter Weibull distribution as follows:

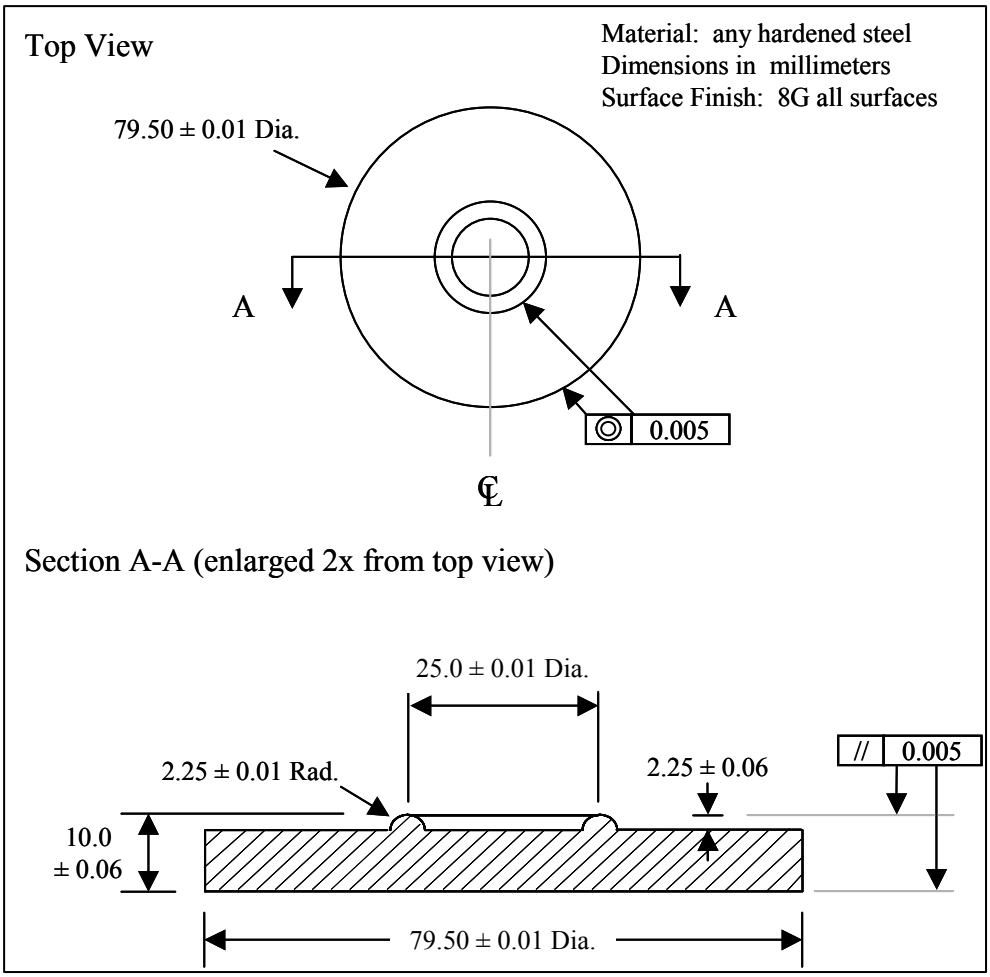

Figure 7. Top- and sectioned-view schematics of the equibiaxial flexure fixture upper ring insert (25-mm diameter).

$$P_f = 1 - \exp\left[-\left(\frac{S}{\sigma_\theta}\right)^m\right], \tag{3}$$

where σ_θ is the characteristic strength and m is the Weibull modulus. The adjective "uncensored" in this context means that each measured strength value has not yet been linked to its strength-limiting flaw type. The characteristic strength is a function of the specimen size; however, its value is related to the material scaling parameter which is a material property for a given strength-limiting flaw type. The Weibull modulus is also a material property for a given strength-limiting flaw type. Greater details of the Weibull distribution and its reporting practices for ceramics may be found in ASTM C1239 (*15*). The parameters σ_θ and *m* were determined using the CERAMIC computer program (*16*) using maximum likelihood estimation (with unbiasing factors) along with 95% confidence bounds about both parameters.

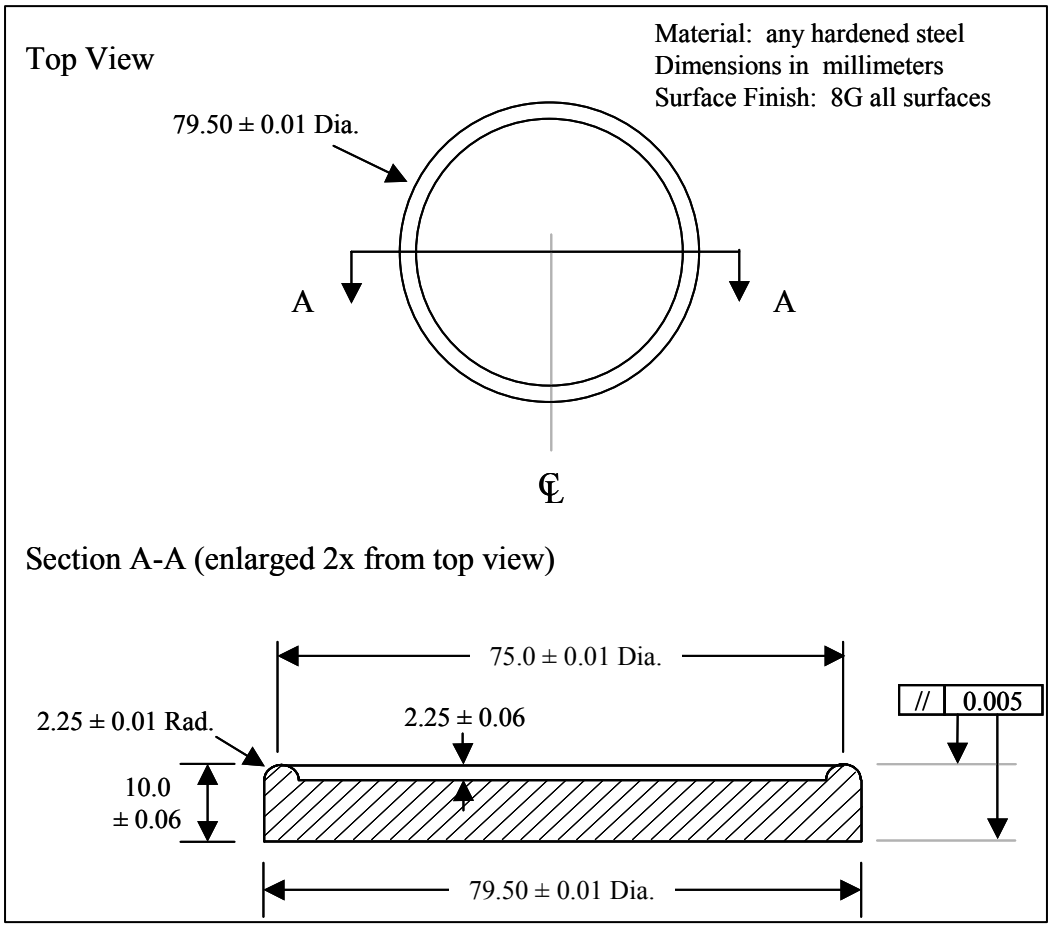

Figure 8. Top- and sectioned-view schematics of the equibiaxial flexure fixture lower ring insert (75-mm diameter).

2.4.2 Fractography

The identification of the strength-limiting flaw type was sought in selected uniaxial flexure specimens for each of the five surface conditions (see table 2). Practices outlined in ASTM C1322 (*17*) were adhered to. Additionally, the examination of strength-limiting flaw types also occurred with the unchamferred uniaxially flexure specimens. Lastly, selected equibiaxial flexure specimens from each of the four unique surfaces (i.e., as-fired, as-received, uniaxial surface ground, and rotary surface ground) were examined. The fractography was performed using reflected light optical microscopy (RLOM) or secondary electron imaging with scanning electron microscopy (SE-SEM) or both.

2.4.3 Strength-Size Scaling

Strength-size scaling with surface area (when strength-limiting flaws are restricted to the specimen surface) or volume (when strength-limiting flaws are volumetric in nature) has long been recognized as a characteristic associated with monolithic ceramics. The following

description pertains to strength-size scaling analysis associated with surface area; analogous analysis associated with volume is not presented.

When surface flaws are strength-limiting, the Weibull distribution for strength-size scaling is represented by

$$P_f = 1 - \exp\left[- k_A A \left(\frac{S}{S_{OA}} \right)^m \right] , \quad (4)$$

where k_A is the area loading factor, A is area of the specimen subjected to tensile stress, and S_{OA} is the area scaling parameter for the material (and has units of MPa·(mm^2)$^{1/m}$). The product of $k_A A$ is typically referred to as the effective area. The loading factor (also called the stress gradient factor) represents the failure stress dependence on the specimen configuration and the (tension) loading conditions. The loading factor has a range of $0 < k_A \leq 1$; it is equal to one only for pure uniaxial tension; and is a function of the Weibull modulus when $k_A < 1$. The loading factor dependence on m is analytic for simple test geometries and loadings, but its calculation and dependence on m requires numeric determination for complex shapes, loadings, or service boundary conditions. The trend of equation 4 shows that higher probabilities of failure exist when greater surface area of a ceramic is subjected to the same tensile stress.

The effective area for an ASTM C1161 Type "B" specimen $(k_A A)_{1161B}$, is (*18*),

$$(k_A A)_{1161B} = \frac{m+2}{2(m+1)} \left[b L_L + \frac{h L_L}{m+1} \right] \quad (\text{units} = \text{mm}^2), \quad (5)$$

where *b* is the specimen width (4 mm), *h* is the thickness or height (3 mm), and L_L is the lower loading span (40 mm). The effective area for an ASTM C1161 Type "B" specimen is illustrated in figure 9 as a function of Weibull modulus (m).

A multiaxial stress state obviously exists in equibiaxial flexure testing, and the calculation of the effective area is more complex since an assumption regarding the effect of a multiaxial fracture criterion must be considered. Batdorf (*19*) and Breder et al. (*20*) considered this, and combining that analysis with the fixture geometry used in the present study, results in the following relationship for the effective area for a ring-on-ring, $(k_A A)_{ROR}$, equibiaxially tested specimen:

$$(k_A A)_{ROR} = 2\pi r_U^{\,2} m^{0.45} = 981.7 m^{0.45} \quad (\text{units} = \text{mm}^2), \quad (6)$$

where r_U is the radius of the upper loading ring (25 mm in this study). The effective area for this equibiaxial flexure testing as a function of Weibull modulus is illustrated in figure 10.

For the same strength-limiting surface flaw, the failure stresses of the two specimen geometries may be related according to

$$\frac{S_{1161B}}{S_{ROR}} = \left[\frac{(k_A A)_{ROR}}{(k_A A)_{1161B}} \right]^{1/m} . \quad (7)$$

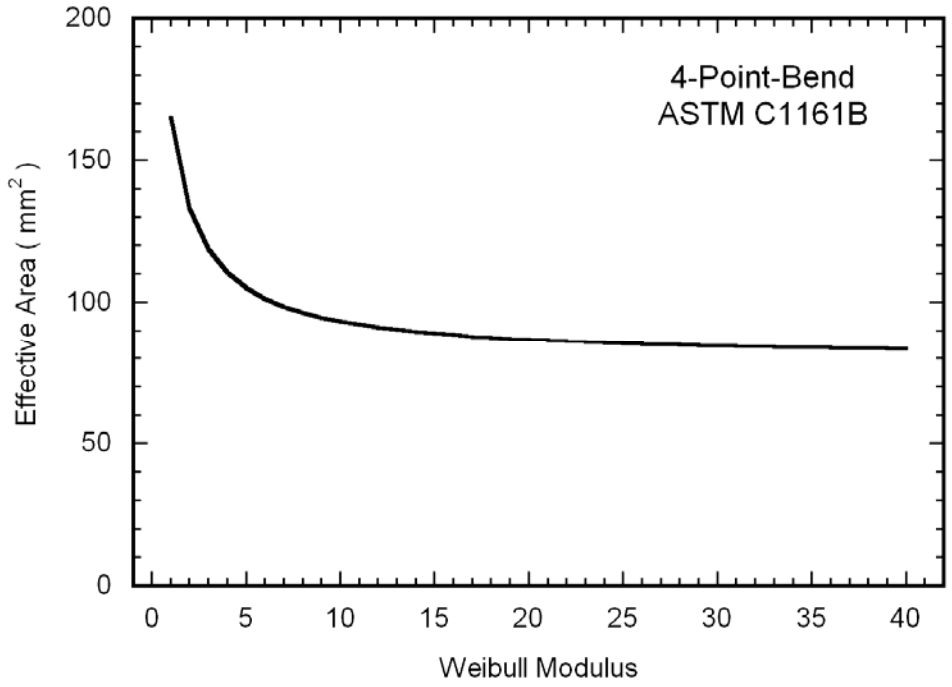

Figure 9. The effective area for the ASTM C1161 type "B" specimen uniaxial flexure specimen as a function of Weibull modulus.

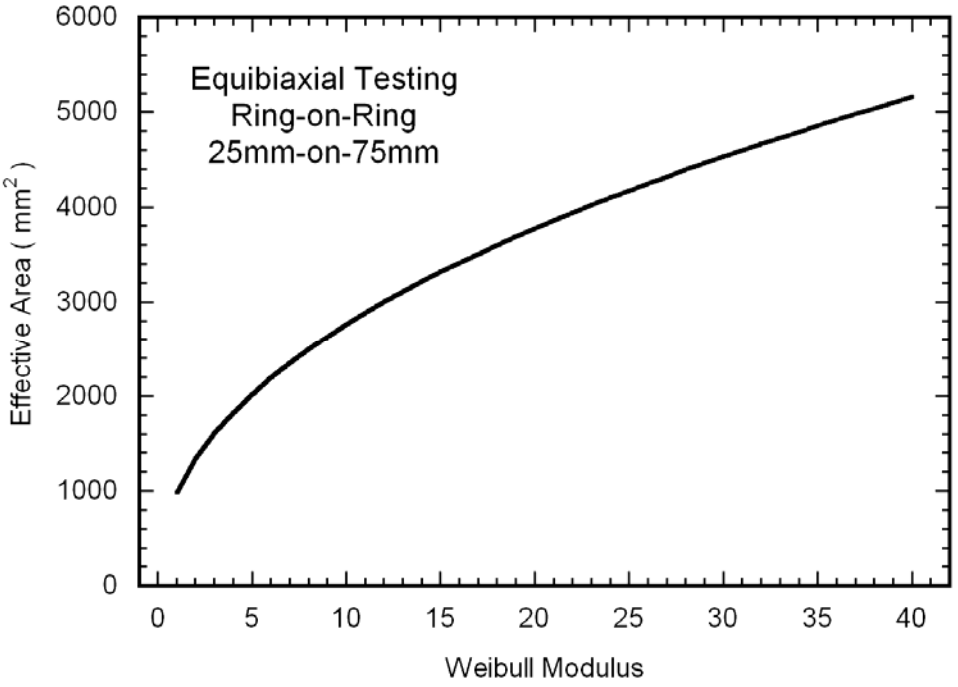

Figure 10. The effective area for the utilized equibiaxial flexure test as a function of Weibull modulus according to equation 6. This expression is only representative for the equibiaxial fixture geometry used in the present study (i.e., upper ring diameter of 25 mm) and Batdorf's multiaxial fracture criterion (*19*).

The percentage of the failure stress for the equibiaxial flexure strength to that of the uniaxial flexure strength is illustrated in figure 11 as a function of Weibull modulus. For example, for a ceramic that has a Weibull modulus of 20, the equibiaxial failure stress (for the test geometry used in the present study) will be ~80–83% of the uniaxial failure stress for any given failure probability.

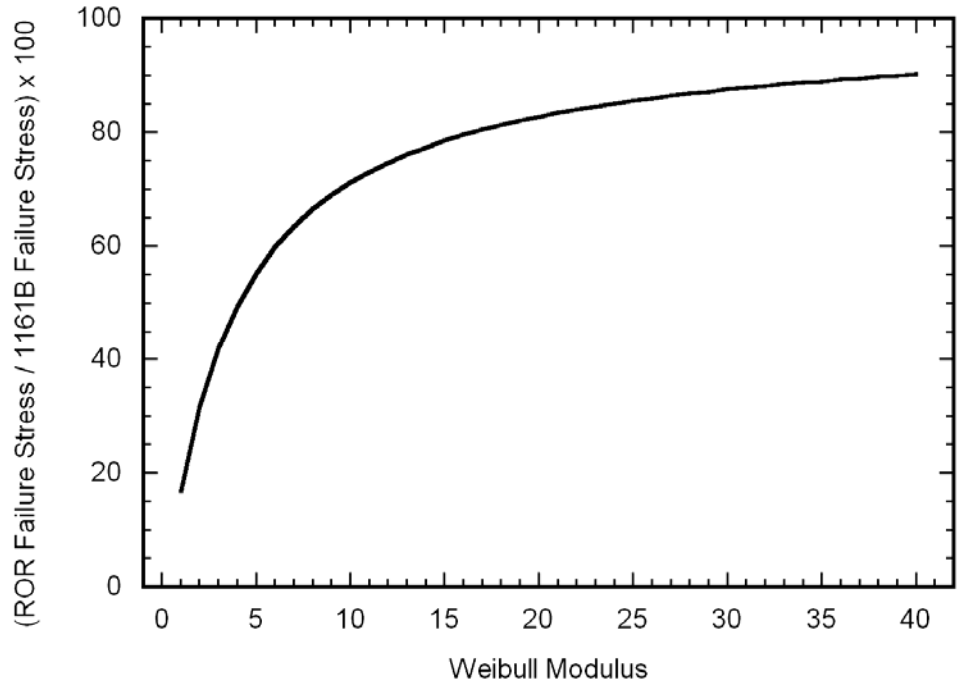

Figure 11. Percentage of the failure stress for the equibiaxial flexure to that of the uniaxial flexure failure stress.

CoorsTek reports (see table 1) an ASTM F417 (*21*) uniaxial flexure strength of 379 MPa for CAP3 AD-995 alumina; however, this strength value, if not strength-size-scaled to the more commonly referred to ASTM C1161 type "B" specimen, appears relatively high and can be misleading. For example, if the F417 strength of CAP3 AD-995 alumina was limited by surface flaws and had a Weibull modulus of 20, then its effective area would only be 2.28 mm^2, and its scaling to ASTM C1161 type "B" specimen using equation 7 show that its expected strength would be only 316 MPa (a 20% decrease).

An issue worthy of greater discussion is the proper utilization of equations 4–7 which is predicated on the fact that *inherently-surface distributed* flaws are the strength limiting features. This may appear to be a moot point; however, the semantics of flaw-type vs. flaw-location can cause confusion if their differences are not understood. For example, a cluster of abnormally large grains located in the interior of a specimen or component is considered an inherently-volume distributed flaw located in the volume. If that same flaw type is located at the surface of a specimen or component, it is still an inherently volume-distributed flaw, but now it is now

located at the surface due to the random nature of the manufacturing or machining process or both. When an inherently-volume flaw is located at a surface (a two-dimensional [2-D] domain) or at an edge (a one-dimensional domain), equations analogous to equations 4–7 for surfaces must be utilized. Similarly, when an inherently-surface distributed flaw (a 2-D entity that cannot be located within the volume, e.g., machining damage or pits due to oxidation or corrosion) is located at an edge, then equations 4–7 would be used. Edge-type flaws are unique in that they can only be located at edges, and analogous equations to equations 4–7 for edges would be used for component design when the component has edges. A temptation of data censoring is to solely censor strength data based on flaw location rather than flaw type (the latter is much more laborious to identify). Though the identification of the flaw location is useful to know, this information is insufficient as input for established probabilistic design and life analysis. Strict data censoring was outside the scope of the present study, so the strength-size scaling analysis conducted (i.e., equations 4–7) among the two test geometries assumed that surface-type flaws (i.e., those generated from machining) were strength-limiting.

3. Results and Discussion

3.1 Microstructural Characterization of CAP3 AD-995

The CAP3 AD-995 has a purity of 99.5%, a density of 3.90 g/cm^3, a reported flexure strength of 379 MPa, an elastic modulus of 370 GPa, a Poisson's ratio of 0.22, a hardness of 14.1 GPa (Knoop-1kg), and a fracture toughness between 4-5 MPa$\sqrt{m}$. The authors ran numerous tests and determined: average density of the material to be 3.88 g/cm^3; average elastic modulus to be 377 GPa by impulse excitation of vibration (*22*) and 381 GPa by pulse-echo (*23*); average Poisson's ratio to be 0.236 by impulse excitation of vibration (*22*); and an average 1000-g Knoop hardness to be 14.9 GPa.

CoorsTek reports an average grain size of 6 μm and a consistent average size of 5.7 μm was measured by the authors (via digital image analysis using a method that was verified to generate equivalent results to the linear intercept method); however, these average values are far from a complete portrayal of the microstructure of this ceramic. It is evident upon inspection of the CAP3 AD-995 microstructure shown in figure 12 that the majority of this volume is occupied by grains that are much larger than 5.7–6.0 μm. Polished sections from randomly selected tiles were inspected, and this microstructure was consistently observed in all. A polished microstructure of AD-995 is shown in figure 13. It is clear that this microstructure is quite different than that of CAP3 AD-995, shown in figure 12a. Further grain size distribution analysis (of 375 counted grains) of the CAP3 AD-995, see distribution in figure 14, showed that 6.6 % of the grains were larger than 15 μm yet occupy 51% of the volume, and 14% of the grains are larger than 10 μm yet occupy 70% of the volume. The grain size distribution of CAP3 AD-995 is much wider than that for AD-995, as also shown in figure 14. Because most of the

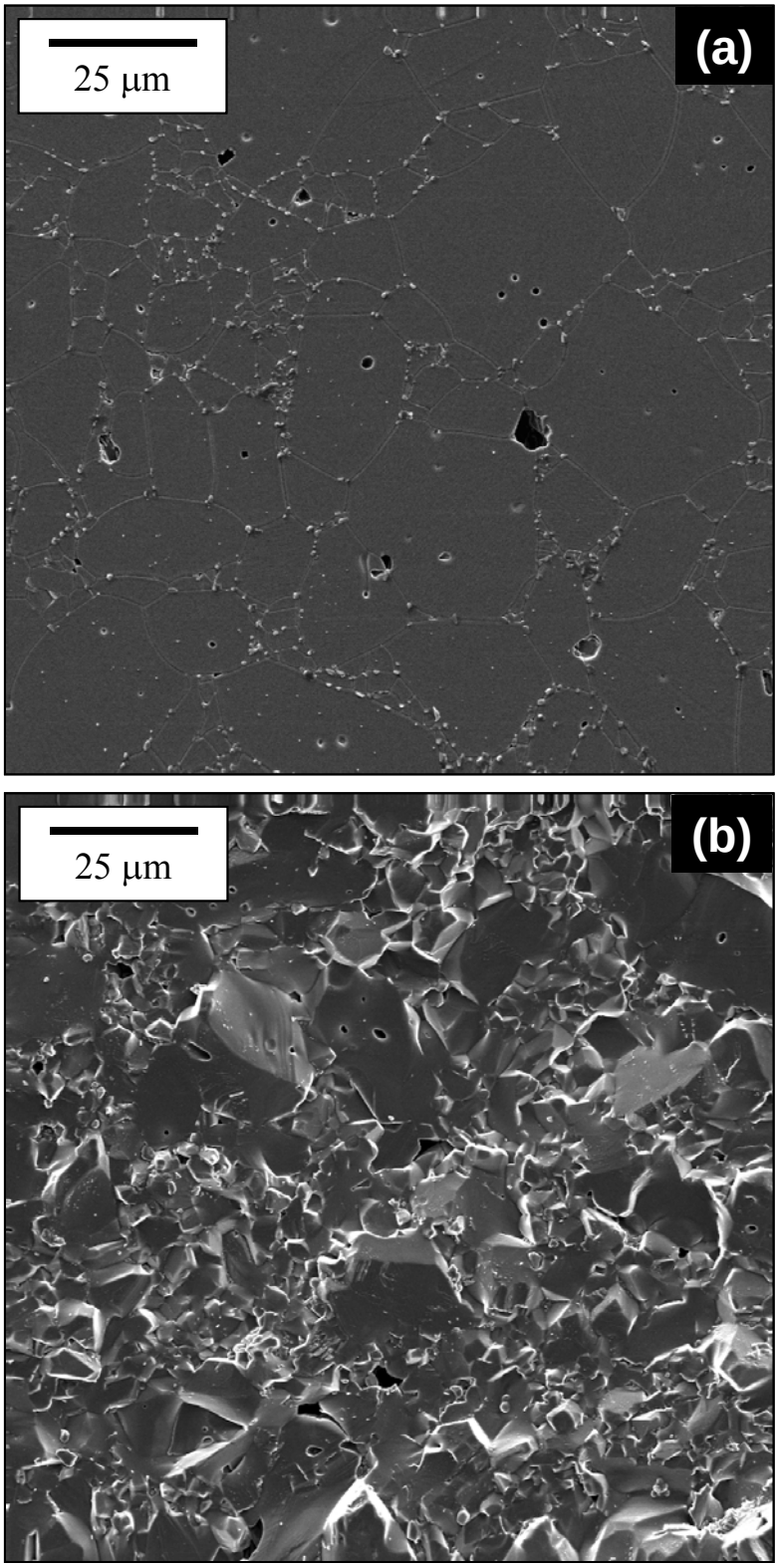

Figure 12. CAP3 AD-995 Al_2O_3 microstructure on a (a) polished and thermally-etched and (b) fractured surface. The latter image shows that transgranular fracture is more dominant than intergranular fracture.

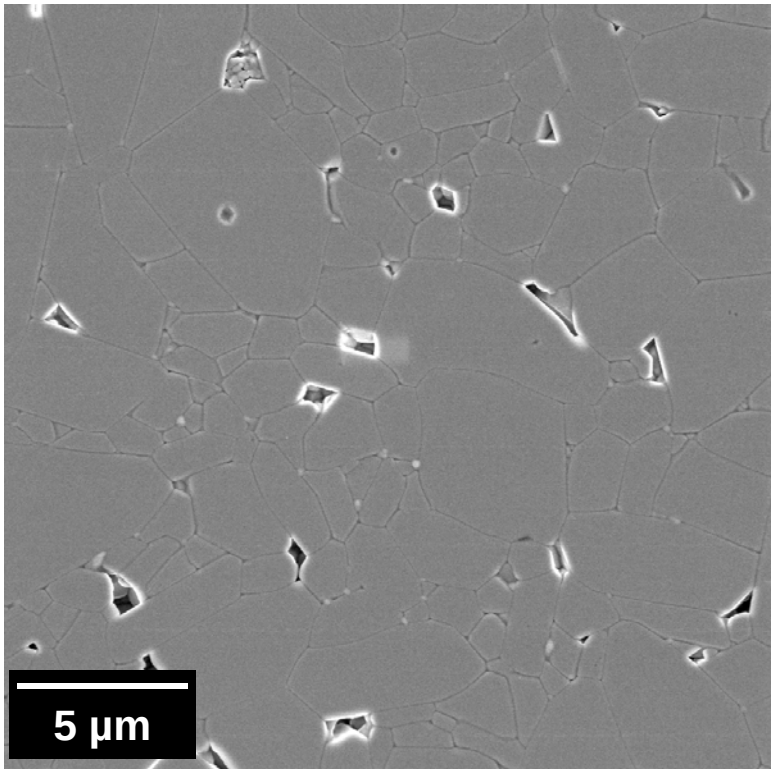

Figure 13. AD-995 Al_2O_3 microstructure—polished and thermally-etched. Though this 99.5%-purity alumina is compositionally equivalent to the CAP3 AD-995 Al_2O_3 tested in this study, its grain size is noticeably smaller (compare to figure 12a).

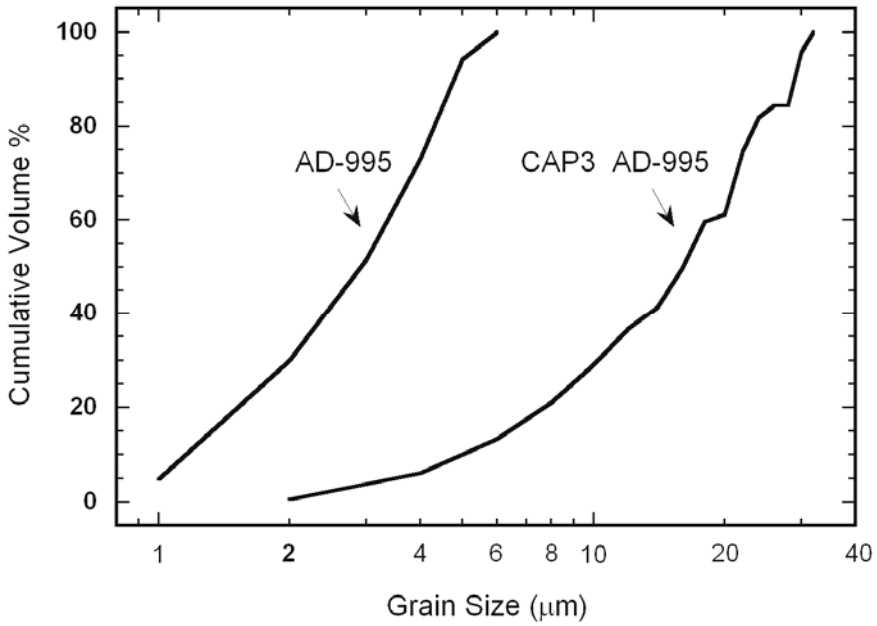

Figure 14. Measured grain size distribution of CAP3 AD-995 (375 grains counted) and AD-995 (166 grains counted).

actual grains in CAP3 AD-995 comprise a small volume of the total bulk, this manifests itself into an average grain size that is misleadingly small. Furthermore, CoorsTek reports an average grain size of 6 μm for the AD-995 alumina (see table 1), whereas the present study measured a much smaller average value of 1.5 μm (166 grains counted). Somewhat hidden in either the CoorsTek information or the present study is that the AD-995 has a much narrower grain size distribution than the CAP3 AD-995 alumina. This is a good illustration of how the meaning of an average grain size value can be an incomplete (or even misleading) microstructure descriptor—especially when the distribution about it is relatively wide.

Unfortunately, confusion results from inspection of the literature as it appears that AD-995 and CAP3 AD-995 are often generically reported as "AD-995" (unfortunately this confusion is reinforced by CoorsTek reporting the exact same properties for both grades), so it is difficult (if not impossible) for readers to discern (unless microstructural images appear in their text) which of the two CoorsTek 99.5% alumina grades was interrogated when "AD-995" is the only description given. The understanding of the differences between these two "AD-995" aluminas is important as the AD-995 alumina is omnipresent in the structural ceramic literature whereas CAP3 AD-995 is somewhat relegated to the armor community. The authors suspect that the differences between these two "AD-995" alumina are often taken for granted, and that the "AD-995" that is sometimes ballistically or high-strain-rate tested is actually the non-armor grade 99.5% alumina. That suspicion unfortunately cannot be supported nor denied though, unless grain size distribution information or microstructures accompany any of the results from those studies.

3.2 Strength as a Function of Surface Condition

Strength depended on surface condition both for uniaxially (figure 15) and equibiaxially (figure 16) tested specimens. Surfaces that were uniaxial or rotary ground using 320-grit diamond machining generated the highest strengths followed in descending order of strengths from as-fired surfaces, and then strengths from surfaces produced by CoorsTek's standard grinding procedure as seen in table 3. Those differences in strengths are statistically significant with 95% confidence. These results show 320-grit machining can increase flexure strength, and suggest that CoorsTek's standard surface grinding procedure of CAP3 AD-995 tiles is perhaps too aggressive if strength-retention is required.

The extra cost of machining CAP3 AD-995 alumina, and the effect on strength, are somewhat enigmatic. First, though CoorsTek's "standard" machining will provide a tile whose dimensions will have stricter tolerances than those of "as-fired" tiles, the extra cost of $14/tile comes at the expense of lower flexure strengths—a 7–8% decrease. The strength of 320-grit machined tiles was 6% and 15% greater than tiles with as-fired surfaces and CoorsTek "standard" ground surfaces, respectively, but that resulted from an additional expense of $45/tile. If desire remains to have CoorsTek perform the surface machining of their CAP3-AD995 alumina tiles and strength-reduction is not allowable, then a requested combination of a less aggressive machining

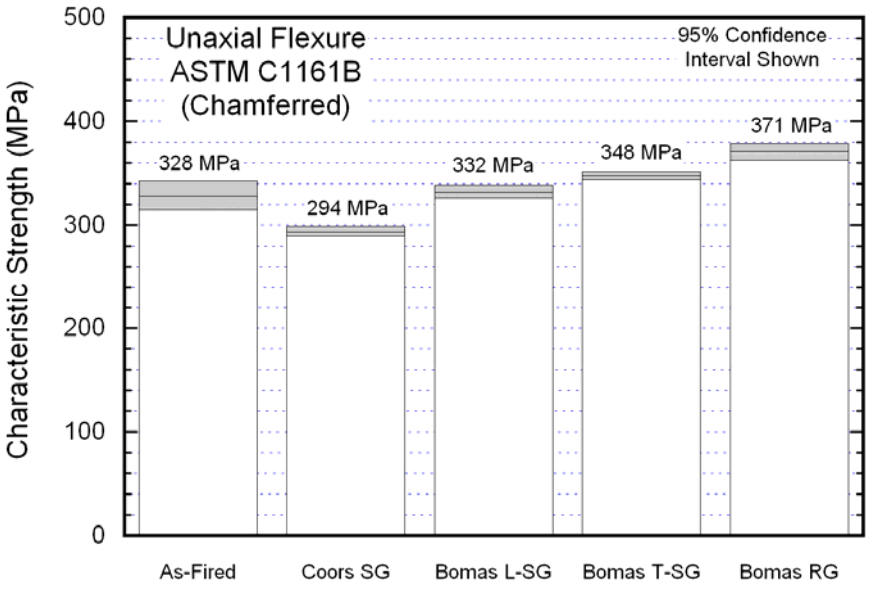

Figure 15. Comparison of CAP3 AD995 characteristic strengths for uniaxial flexure tests of specimens with chamfered edges. SG = surface ground; RG = rotary ground; L = longitudinally ground; and T = transversely ground.

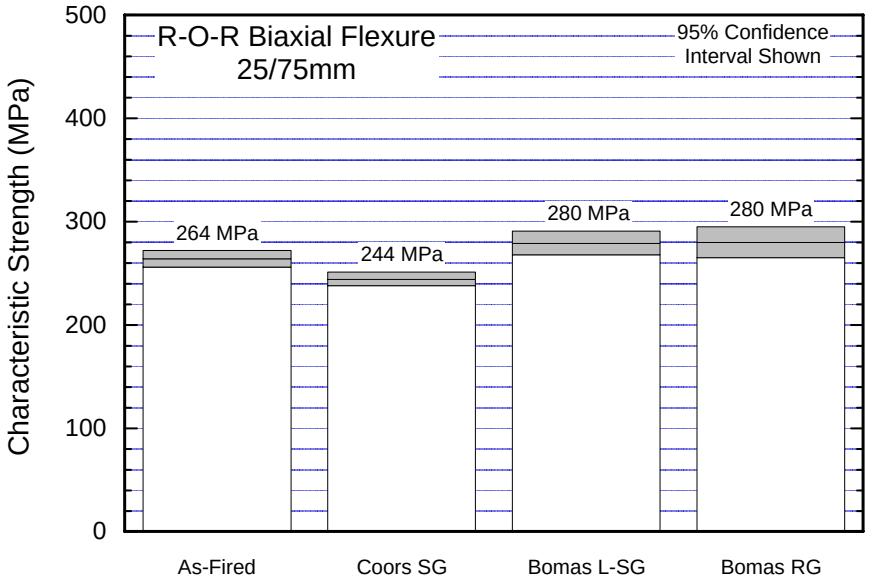

Figure 16. Comparison of CAP3 AD995 characteristic strengths for equibiaxial flexure. SG = surface ground; RG = rotary ground; L = longitudinally ground; and T = transversely ground. Bomas L-SG and Bomas T-SG are equivalent for equibiaxial flexure testing.

Table 3. Two-parameter Weibull strength distributions and their 95% confidence estimates.

Surface Condition	Test Type	No. of Tests	Relative Humidity (RH) (%)	Uncensored Characteristic Strength, σ_θ [± 95% Conf. Est.] (MPa)	Uncensored Weibull Modulus, m [± 95% Conf. Est.]
As-fired	Uniaxial - chamfer	30	55	328 [315, 343]	8.8 [6.3, 11.9]
	Uniaxial - no chamfer	30	44	310 [301, 319]	13.3 [9.8, 17.3]
	Equibiaxial	13	[a]	264 [256, 272]	19.6 [12.1, 29.0]
As-received	Uniaxial - chamfer	30	55	294 [290, 299]	23.7 [17.1, 31.4]
Rotary ground	Uniaxial - no chamfer	30	62	283 [279, 287]	26.5 [19.6, 34.5]
(80-grit)	Equibiaxial	6	[a]	244 [238, 251]	39.9 [18.9, 69.5]
Longitudinal	Uniaxial - chamfer	28	55	332 [326, 339]	20.4 [14.8, 27.0]
Transverse	Uniaxial - chamfer	28	35	348 [344, 352]	33.6 [24.7, 43.6]
	Equibiaxial	6	[a]	280 [268, 291]	25.4 [11.9, 45.2]
Rotary	Uniaxial - chamfer	27	34	371 [363, 379]	18.4 [13.1, 24.8]
Ground	Uniaxial - no chamfer	27	62	343 [337, 349]	24.1 17.3, 32.0]
(320-grit)	Equibiaxial	6	[a]	280 [265, 295]	19.6 [9.2, 35.0]

[a] RH was inadvertently not measured when the equibiaxial flexure tests were conducted; however, they were all tested on the same day (and believed to have been subjected to the same RH).

practice and a finer grit grinding wheel should be made by the customer. Clearly, the 320-grit machining procedure benefits strength; however, the extra expense for machining is hardly justified by the relatively low amount of strengthening.

As expected, chamfered edges on specimens had a beneficial effect on uniaxial flexure strength. *Not* chamfering uniaxial flexure specimens resulted in a strength reduction of ~4–8% for a given machining condition, see figures 17–21 and table 3. The reduction in strength correlated with failure consistently initiating at the edge of these specimens (an occurrence not observed when bend bar edges were chamfered). A lack of edge chamfering inherently has no effect on centrally loaded equibiaxial flexure strength. It may have an affect if the tile is mechanically loaded close to an edge and that edge is unchamferred. Chamfering edges in ceramic specimens and components has been long recognized to increase strength. In spite of that recognized effect, the study of chamfered or unchamferred edges in the present study was revisited because ceramic tiles for most armor applications are commonly purchased with unchamferred edges and interest therefore existed to statistically illustrate their detrimental effect on strength.

Uniaxial flexure testing with ASTM C1161-94 also produced strengths that were dependent upon machining direction, whereas equibiaxial flexure strengths were inherently independent of the machining direction because of the nature of its associated stress state. The directional-dependence on uniaxial flexure strength was a consequence of the interaction between the extent of anistropic machining damage and the relatively large average grain size of the CAP3 AD-995 alumina. Though directional dependence on uniaxial flexure strength was anticipated, it was expected that the uniaxial flexure strength of the longitudinally-machined ASTM C1161 type

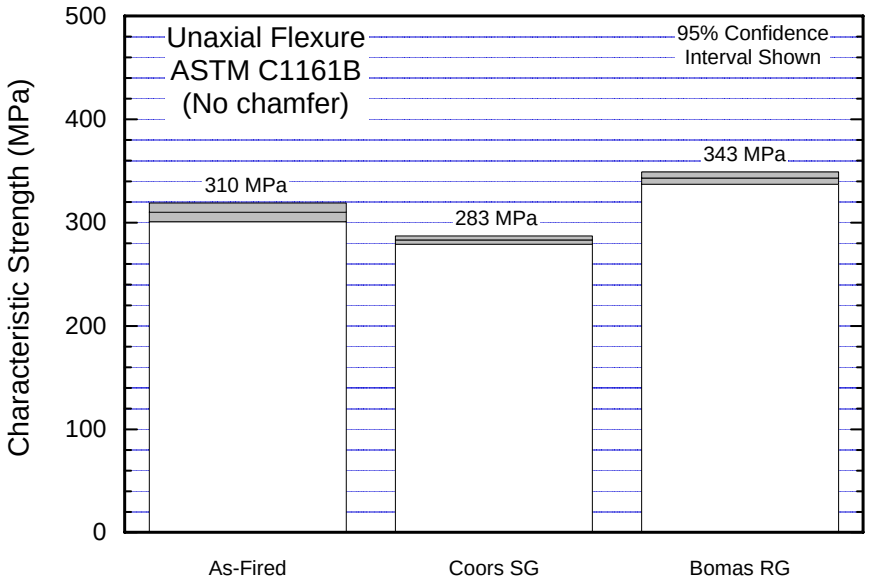

Figure 17. Comparison of CAP3 AD995 characteristic strengths for uniaxial flexure tests of specimens without chamfered edges. SG = surface ground and RG = rotary ground.

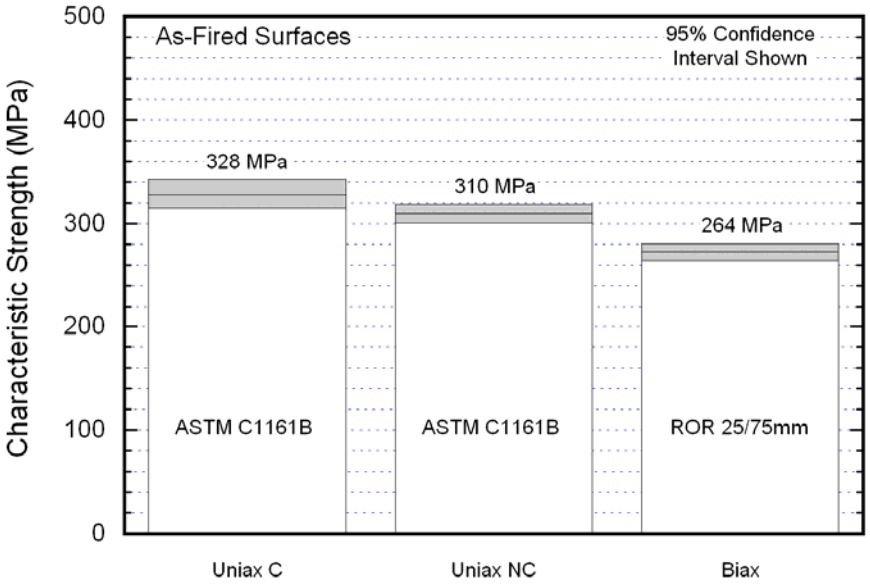

Figure 18. Comparison of CAP3 AD995 characteristic strengths for the three different test types for specimens with as-fired surfaces.

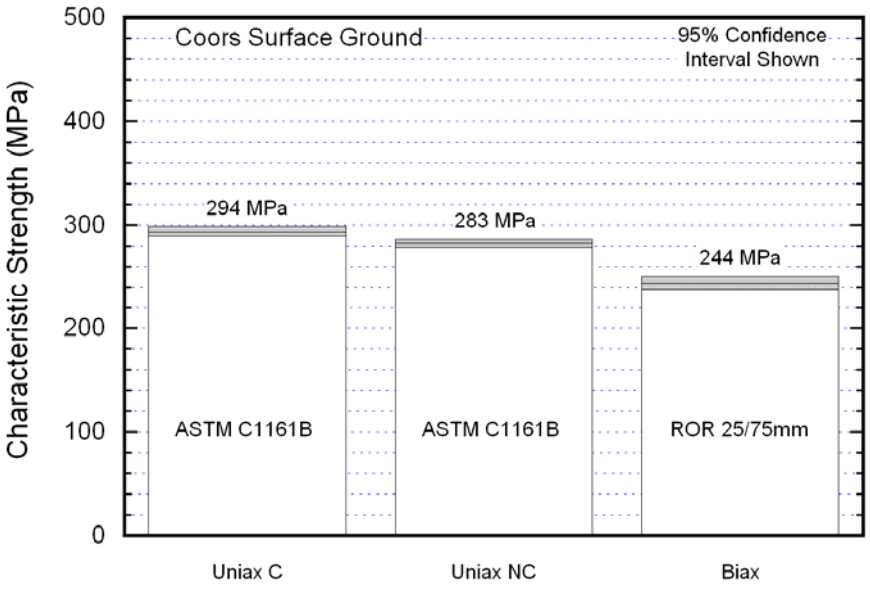

Figure 19. Comparison of CAP3 AD995 characteristic strengths for the three different test types for specimens with as-received (80-grit surface ground) surfaces.

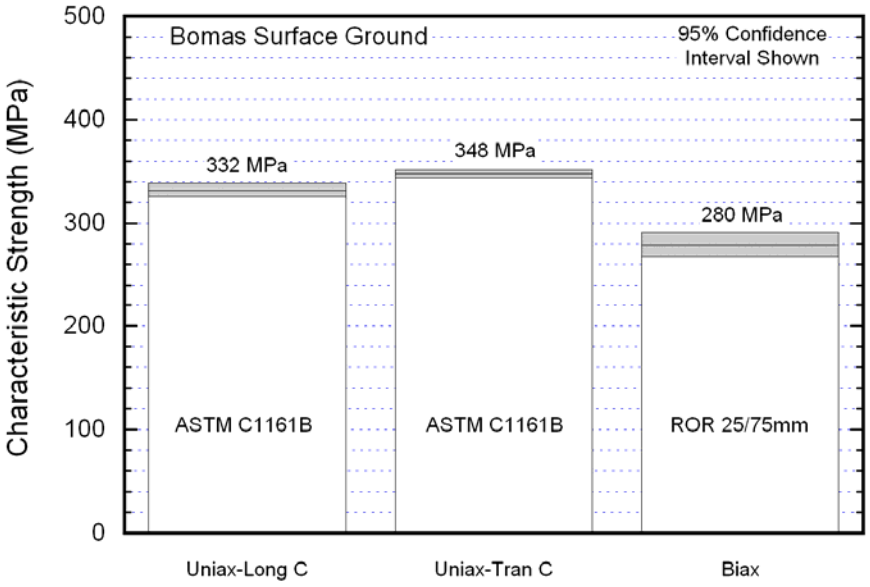

Figure 20. Comparison of CAP3 AD995 characteristic strengths for longitudinally and transversely machined (chamfered) ASTM C1161 type "B" bend bars and equibiaxial tested tiles with 320-grit surface ground surfaces. The effect of chamfering was not explored with this surface condition.

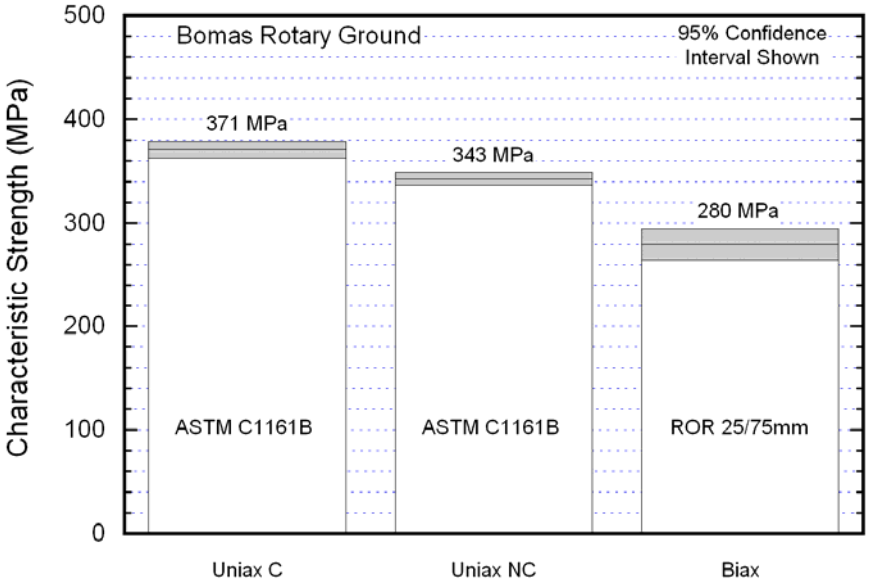

Figure 21. Comparison of CAP3 AD995 characteristic strengths for the three different test types for specimens with rotary ground (320-grit machined) surfaces.

"B" specimen would be larger than that for transversely-machined bars as the literature is densely populated with such observations for fine-grained polycrystalline ceramics (*24–27*); however, the opposite trend was observed with this coarse-grained alumina. The directional-dependence of uniaxial flexure strength only complicates the general interpretation of flexure strength's dependence on surface condition. Whereas equibiaxial flexure testing facilitates surface condition comparisons because of its "averaging effect" on machining directionality—it is perhaps a better flexure test for assessing flexure strength of armor tiles.

Rice (*28*, *29*) found for a variety of ceramics that the ratio of transversely-ground strengths to longitudinally-ground strengths exhibited a maximum when those ceramics had a relatively large average grain size. For example, the ratio of the two strengths was reported to be close to unity when alumina had an average grain size of ~20 μm, and the ratio decreased when the average grain size was both finer and coarser than that size. Rice attributed this maximum ratio of 1 to be a consequence of the strength-limiting flaw size (more specifically, the flaw shape) to be constrained by the (relatively large) grain size. Machining-induced flaws in fine-grained ceramics tend to have semi-elliptical-shaped flaws that are larger than the average grain size. In larger-grained ceramics, the shape of the machining flaw is influenced by the grain size. Depending on the grain-size/flaw-size interaction it is possible to have semi-elliptical machining flaw entirely contained in a single grain. In this case the strength will be affected by the orientation of the machining flaw to the crystallographic orientation of that grain.

Residual stresses due to machining were considered as a possible source of the strength difference. Machining produces a compressive residual stress field on surfaces with greater

compressive stresses perpendicular to the grinding direction than parallel with it (*30*). Piezoluminescence measurements on the ground surfaces of selected specimens from all five test specimen sets showed that the residual compressive stresses were relatively small in magnitude (see table 4) for all the different surface conditions and could not be used to reconcile the differences in characteristic strengths. For example, if one set had a characteristic flexure strength of 400 MPa with no residual compressive stresses on the tensile surface, and a second set had a characteristic flexure strength of 500 MPa with a residual compressive stress of 100 MPa, then it is the presence of the residual compressive stress on the latter set that results in the higher flexure strength. The characteristic strength differences among investigated sets were on the order of many tens of MPa, whereas the differences in the compressive residual stresses among those sets were smaller than that, and therefore cannot be used as an explanation for those differences in characteristic strengths.

Table 4. Surface residual stress measured via piezoluminescence.

Surface Condition	Specimen	Fracture Strength (MPa)	Hydrostatic Stress (MPa)	Hydrostatic Stress Std. Dev. (MPa)
As-fired	AF2	334.0	–5	6
—	AF3	289.3	11	17
—	AF4	357.9	1	15
As-received	AR1	296.0	–12	32
Rotary ground	AR2	303.9	–36	19
(80-grit)	AR3	302.0	–24	23
Longitudinal	L1	327.4	–24	10
—	L2	325.7	–23	11
—	L3	341.3	–21	11
Transverse	T1	352.1	–5	25
—	T2	348.5	–26	25
—	T4	344.2	–11	14
Rotary	R2	346.0	–33	31
Ground	R3	360.4	–16	11
(320-grit)	R4	321.8	–25	17

Note: Tensile surface of bend bars evaluated. Spot size ~2 μm, and penetration depth ~5 μm.

There is evidence that high relative humidity (RH) can result in lower strengths (about a 10% strength decrease between 30% and 60% RH) in fine-grained AD995 alumina (*31*, *32*). None of the five sets in this effort were tested under varying RH (i.e., each set was tested in one-day when RH was presumably unchanged during the testing) so it cannot be concluded that RH affected any of the strengths measured in the present study. Although the alumina examined in this study and the alumina from previous work showing the strength dependence on RH were technically the same, it is not known if the microstructures were equivalent as the other authors did not report such information. This information is an unfortunate omission as average grain size in such commercially available aluminas can vary by almost an order of magnitude. The characteristic strength of the transversely machined set in the present study was ~5% greater than

that of the longitudinally-machined set, and the RH was higher on the day that the latter was tested, so the trends in strength and RH between them are consistent with findings from the work of Cho et al. (*31*, *32*). The above-described and more completely documented effect of grain size on strength-anisotropy is believed to be the primary cause of the strength differences between the transversely and longitudinally machined sets.

3.3 Strength-Limiting Flaws

The measure of the flaw origin size, a, (i.e., depth of a surface flaw) can be estimated using the Griffith equation,

$$a = \left[\frac{K_{Ic}}{\sigma Y} \right]^2 \quad , \tag{8}$$

where K_{Ic} is the fracture toughness, σ is the fracture stress at the origin, and Y is a stress intensity shape factor for the origin. If a fracture toughness of 4 MPa√m is considered in equation 8 along with the extreme values of Y associated with circular or semi-elliptical flaw shapes (*17*), then the strength-limiting surface flaw size for the characteristic strengths listed in table 3 should range in size between ~30 and 160 μm. Examples of strength-limiting flaws are shown in figures 22–27 for the five respective surface conditions listed in table 2 and for an unchamferred bend bar. The flaws were almost always volume-type flaws (e.g., agglomerates, regions of large grains) that were located on, or near, the surface and that even appeared to be hybridized with machining damage in those sets that involved machining (i.e., not the as-fired surface condition). Edge failures existed in many of the unchamferred bend bars.

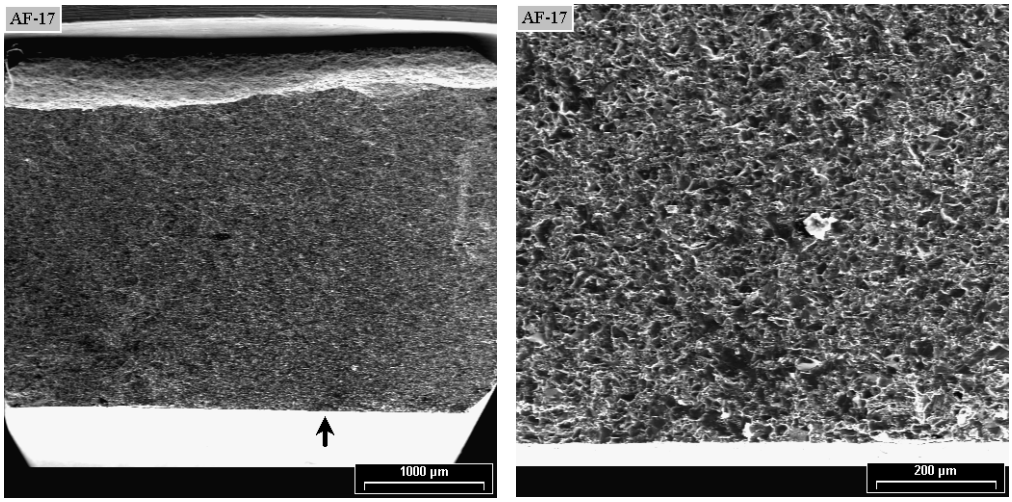

Figure 22. Fracture surface of an as-fired, chamfered, ASTM C1161 type "B" specimen showing (left) failure location and (right) higher magnification image of the location containing the strength-limiting flaw.

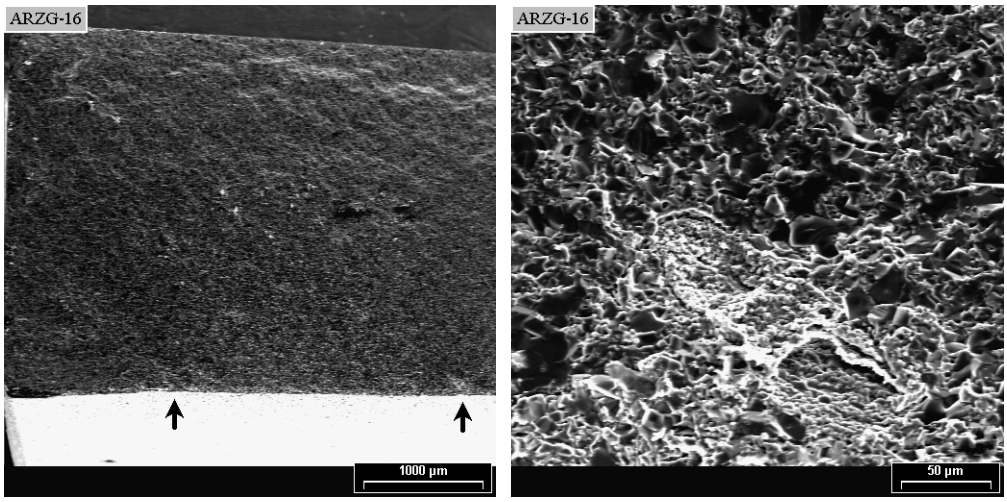

Figure 23. Fracture surface of an as-received, CoorsTek ground, chamfered, ASTM C1161 type "B" specimen showing (left) failure location and (right) higher magnification image of the location containing the strength-limiting flaw. The concave region in the right image may indicate the presence of an agglomerate.

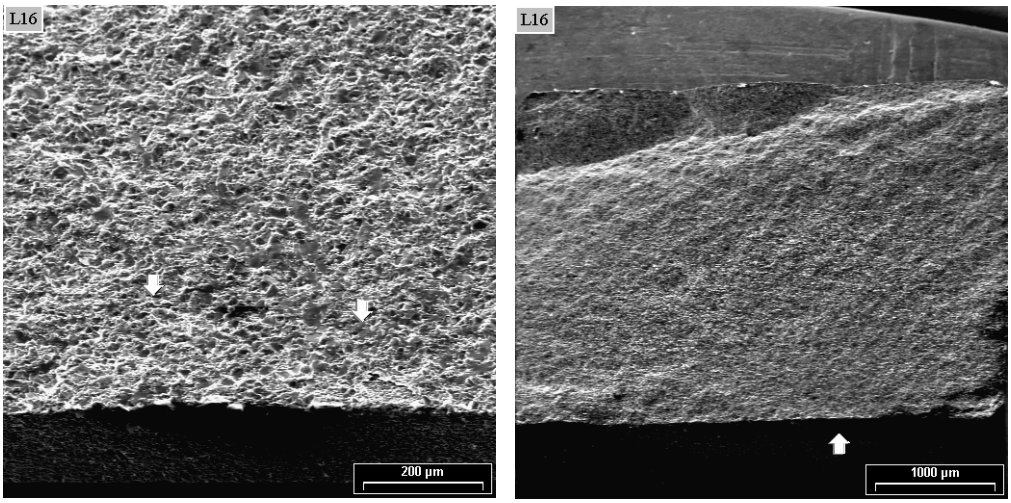

Figure 24. Fracture surface of a longitudinally-ground, chamfered, ASTM C1161 type "B" specimen showing (left) failure location and (right) higher magnification image of the location containing the strength-limiting flaw. Elongated semielliptical flaw typically associated with machining.

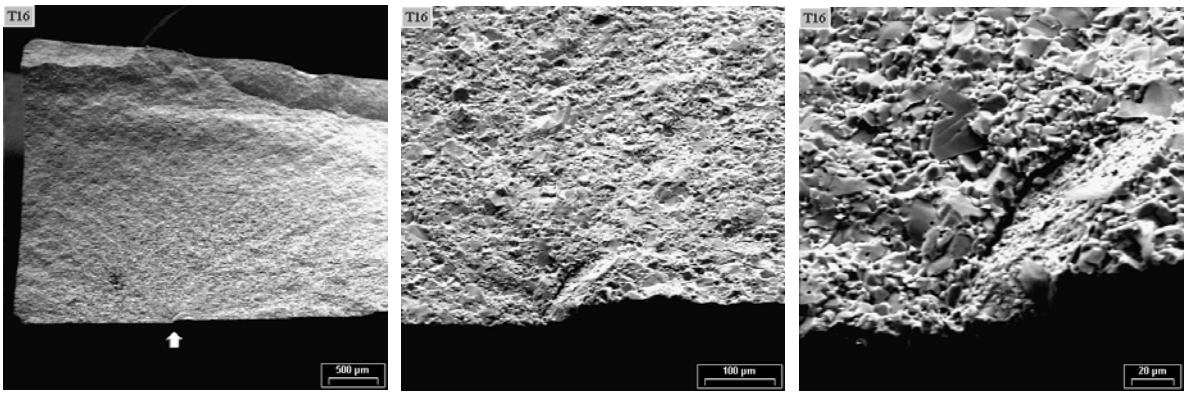

Figure 25. Fracture surface of a transversely-ground, chamfered, ASTM C1161 type "B" specimen showing (left to right) progressively higher magnification images of the location containing the strength-limiting flaw. Origin appears to be cluster of large grains coupled with a porous region.

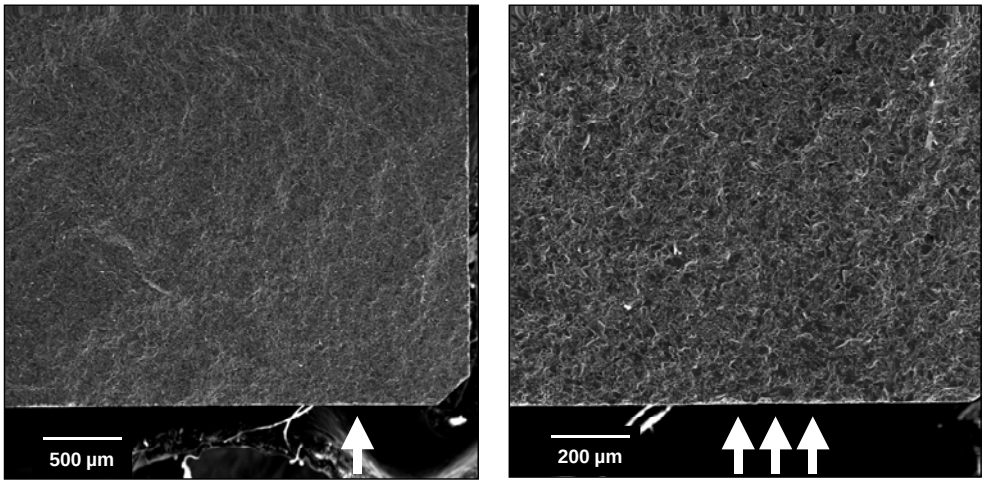

Figure 26. Fracture surface of a rotary-ground, chamfered, ASTM C1161 type "B" specimen showing (left) failure location and (right) higher magnification image of the location containing the strength-limiting flaw. Semielliptical flaw commonly associated with machining damage.

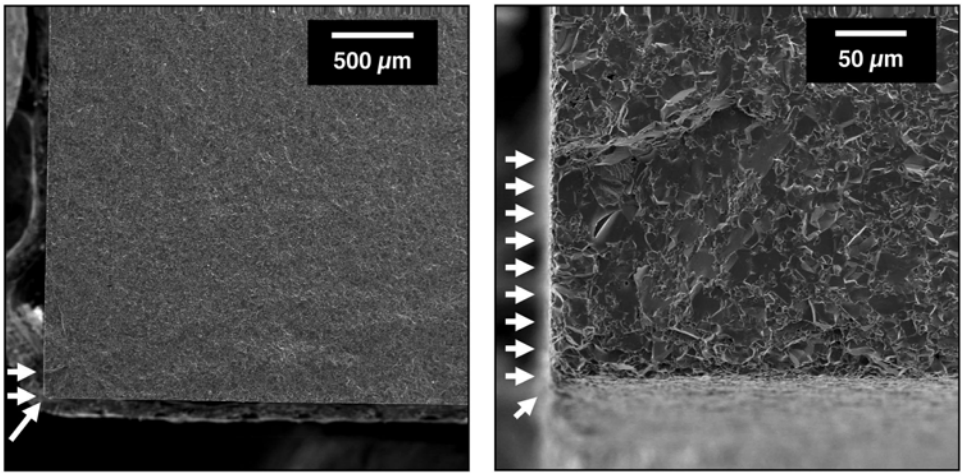

Figure 27. Fracture surface of an As-Received, CoorsTek ground, unchamfered, ASTM C1161 type "B" specimen showing (left) failure at the corner and (right) higher magnification image of the location containing the strength-limiting flaw.

3.4 Strength-Size Scaling

Equibiaxial flexure strengths were ~20% less than uniaxial flexure strengths for any of the four investigated surface conditions. This amount correlates very well with predicted strength-size scaling between the two geometries using Weibull theory and equation 7. Because this failure stress is lower, and probably more representative of on-center ballistic loading of ceramic tiles, its use is perhaps better suited as input in ballistic models that consider such deflections.

3.5 Summary of Strength Results

The results from this study show that machining practices can be employed to increase flexure strength which may be beneficial to the ballistic performance of armor ceramics. Modifying the surface of a ceramic tile to increase the strength will be beneficial to ballistic performance only under certain conditions. These conditions will be met when the combination of tile thickness and impact load (threat) result in tensile-induced cracking of the back face of the ceramic as illustrated in figure 28. This is consistent with other reports describing the nature and chronologies of impact-induced cracking and fracture (*33–36*). Applications where these conditions may be met include body armor and some vehicular armor where relatively thin ceramic tiles may be used (e.g., thin WC tiles in place of thick SiC tiles).

The dependence of tile strength on surface condition may have a different degree of severity for armor ceramics that have a smaller average grain size or that are inherently stronger than CAP3 AD-995 alumina. The size of the grains comprising the majority of the volume in CAP3 AD-995 alumina are of the scale of the calculated strength-limiting flaw size, per equation 8. That will probably not be the case for finer-grained monolithic ceramics that are stronger. Though finer-grit diamond machining increased the strength of CAP3 AD-995 by up to 15% in the present study, an analogous increase in finer-grit machining of a fine-grained monolithic ceramic

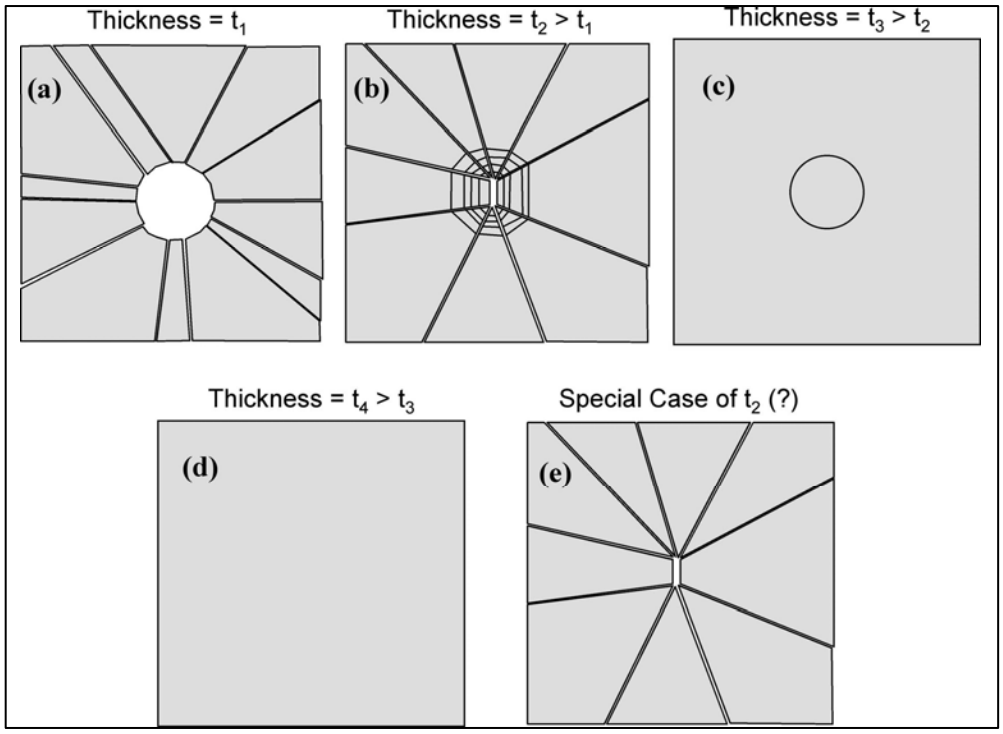

Figure 28. Schematic of fracture pattern trends due to on-center impact (as a function of tile thickness) and their proposed link to equibiaxial flexure testing.

may be more substantial and even sufficient enough to cause the dominant strength-limiting flaw to change as a function of machining condition (*37*). Such a strength dependence on machining should be performed on armor-grade hot-pressed SiCs that are approximately 50% stronger than CAP3 AD-995 and have a grain size distribution with a maximum size less than 10 μm.

From a manufacturing quality control perspective, the equibiaxial flexure test apparatus and method utilized in the present study may potentially be used as a "proof test" to discriminate strong tiles from weak ones. If strong tiles (i.e., tiles that can withstand greater center-line deflection prior to fracturing) could be linked to better ballistic performance, then this equibiaxial flexure test could be used to filter out and eliminate those tiles that have low potential for ballistic performance.

Shock stress wave effects, though affective, are not considered here. Back of the tile shown and impact direction is perpendicular to the shown faces and toward the reader.

- Tile thickness (t) is so thin ($t = t_1$) that the projectile completely penetrates. This is similar in appearance to an invalid equibiaxial flexure test (see figures 4–5). Controlled machining of the ceramic probably will have little or no effect on performance.
- Tile is sufficiently thick ($t = t_2 > t_1$) to achieve partial penetration. Energy of threat is sufficiently high enough to cause concentric conoid patterns on previously created backface-equibiaxial-tension-induced cracks. This too is similar in appearance to an

invalid equibiaxial flexure test (see figures 4–5). Controlled machining of the ceramic may have an effect and perhaps it may be able to promote fracture toward that of the pattern of $t = t_3$.

- Tile is sufficiently thick ($t = t_3 > t_2$) so that backface-equibiaxial-tension-induced cracks are not created; however energy of the threat is sufficient to only drive a single conoid crack through to the backface. Controlled machining of the ceramic probably will have little or no effect on this.
- Tile is thick enough ("semi-infinite," $t = t_4 > t_3$) that no cracks are created on the back face. Controlled machining of the ceramic probably will have little or no effect on this.
- Special case of $t = t_2$: partial penetration was achieved, and the energy of the threat was not sufficient to drive conical cracks through to its surface. Fracture pattern the same as that from valid equibiaxial flexure testings (see figures 4–5).

4. Conclusions

The effect of surface condition on the uniaxial and equibiaxial flexure strength of CoorsTek's CAP3 AD-995 alumina was examined. The following four surface conditions were considered: as-fired (i.e., unmachined); the condition produced by CoorsTek's standard surface grinding procedures (i.e., the surface they will produce on tiles unless otherwise specified); the condition resulting from uniaxial surface grinding with 320-grit diamond machining (i.e., following the machining method specified for ASTM C1161-94 ceramic flexure bars); and rotary surface grinding with 320-grit diamond machining.

Strength depended on surface condition. Surfaces that were uniaxial or rotary ground using 320-grit diamond machining generated the highest strengths (equibiaxial flexure characteristic strength = 280 MPa), followed in descending order of strengths from as-fired surfaces (equibiaxial flexure characteristic strength = 264 MPa), and then strengths from surfaces produced by CoorsTek's standard grinding procedure (equibiaxial flexure characteristic strength = 244 MPa). Those differences in strengths are statistically significant with 95% confidence. These results show that the use of controlled machining procedures to minimize the development of machining-related cracks can increase flexure strength. It also suggests that CoorsTek's standard surface grinding procedure of CAP3 AD-995 tiles is perhaps too aggressive.

The balance of the extra cost of machining CAP3 AD-995 alumina and their effects on strength is subjective. Though CoorsTek's "standard" machining will provide a tile whose dimensions will have stricter tolerances than those of "as-fired" tiles for an extra cost of $14/tile ($4 \times 4 \times 0.118$ in tile geometry), that comes at the expense of a 7–8% decrease in strength. The characteristic strengths of 320-grit machined tiles were 6% and 15% greater than for tiles with

as-fired surfaces and CoorsTek "standard" ground surfaces, respectively, but that came at an additional expense of $45/tile. If the desire remains to have CoorsTek perform the surface machining of their CAP3-AD995 alumina tiles, then a requested combination of a less aggressive machining practice and a finer grit grinding wheel should be considered by the customer if strength retention is deemed important. Clearly, the 320-grit machining benefits strength; however, justification of the extra expense for that relatively low amount of strengthening will need to be made on a case by case basis.

As expected, chamfered edges were observed to have a beneficial effect on uniaxial flexure strength. Chamfering uniaxial flexure specimens resulted in a strength increase of ~4–8% for a given machining condition for CAP3 AD-995 alumina. The lower strength of the unchamfered specimens correlated with failure consistently initiating at the edge of these specimens (an occurrence not observed when bend bar edges were chamfered). A lack of edge chamfering inherently had no effect on equibiaxial flexure strength; however, it may if a tile is mechanically loaded closer to one of its edges (and that edge is chamfered or unchamferred).

Uniaxial flexure testing with ASTM C1161 type "B" specimen produced strengths that were susceptible to machining direction, whereas equibiaxial flexure strengths were not. The directional-dependence on uniaxial flexure strength was a consequence of the interaction between the extent of anistropic machining damage and the relatively large average grain size of CAP3 AD-995 alumina. The directional-dependence on uniaxial flexure strength effect only complicates the general interpretation of flexure strength's dependence on surface condition, whereas equibiaxial flexure testing facilitates surface condition comparisons because of its "averaging effect" on machining directionality—it is perhaps a better flexure test for assessing flexure strength of armor tiles.

Equibiaxial flexure strengths were ~20% less than uniaxial flexure strengths for all of the four investigated surface conditions. This amount correlates very well with predicted strength-size scaling between the two geometries using the Weibull theory. Because this failure stress is lower, and probably more representative of on-center ballistic loading of ceramic tiles, its use is conservative and perhaps better suited as input for ballistic models that consider such deflections.

The results from this study show that machining practices can be employed to increase flexure strength which may have beneficial ramifications on ballistic performance. Issues of flexure strength dependence on surface condition are likely to be more relevant under certain combinations of tile thickness and impact load (threat) (i.e., body armor and some vehicular armor applications). Similar testing should be conducted on the stronger, finer-grained SiC armor ceramics, since the affect of machining on flexure strength may be more pronounced.

In addition to the affect of machining on strength, this study revealed an often-overlooked issue with AD-995. CoorsTek manufactures and markets two grades of compositionally equivalent, 99.5%-purity alumina which they have designated as AD-995 and CAP3 AD-995. The latter was tested in the present study. CoorsTek reports identical properties and average grain size for

these two 99.5% grades (an average size of 1.5 and 5.7 μm, respectively, was measured for AD-995 and CAP3 AD-995 in the present study). Although these values may be statistically correct in their measurements, the narrow and wide grain size distributions of AD-995 and CAP3 AD-995 respectively, are not illustrated by that mean value. It is in the investigator's interest to understand the grain size distribution of the 99.5%-pure Al_2O_3 under investigation and to recognize which of the two grades that they are actually interrogating (it would be wise to understand the grain size and microstructure irrespective of the purity level). If that information is suspect, and results have differences from those from other studies involving 99.5%-purity aluminas, then the possible (and potentially simple) explanation for those differences may be lost.

5. References

1. ASTM C1161-94. Standard Test Method for Flexure Strength of Advanced Ceramics at Ambient Temperatures. *Annu. Book ASTM Stand.* **2001**, Vol. 15.01.
2. MIL-P-46199 (MR). *Plate: Aluminum Oxide Ceramic (For Use in Armor Composites).* June **1989**.
3. Armor Products. CoorsTek, www.coorstek.com, 2001.
4. Material Properties Standard 2000. CoorsTek, www.coorstek.com, 2001.
5. Foster, J. CoorsTek. Private communication, October 2000.
6. Wallace, J. S.; Fuller, E. R., Jr.; Freiman, S. W. Mechanical Properties of Aluminum Nitride Substrates. Report NISTIR 5903, U.S. Department of Commerce, 1996.
7. Ritter, J. E.; Jakus, K.; Batakis, A.; Bandyopadhyay, N. Appraisal of Biaxial Strength Testing. *Journal of Non-Crystalline Solids* **1980**, *419-24*, 38–39.
8. Wereszczak, A. A.; Kirkland, T. P.; Breder, K.; Lin, H.-T.; Andrews, M. J. Biaxial Strength, Strength-Size-Scaling, and Fatigue Resistance of Alumina and Aluminum Nitride Substrates. *International Journal of Microcircuits and Electronic Packaging* **1999**, *22*, 446–458.
9. ASTM F394. Standard Test Method for Biaxial Flexure Strength (Modulus of Rupture) of Ceramic Substrates, *Annu. Book ASTM Stand.* **1998**, Vol. 10.04.
10. Cimpoeru, S. J. The Durability Aspects of Armouring With Ceramic Tiles. *Journal of Materials Science Letters* **1996**, *15*, 837–39.
11. ASTM C1499. Standard Test Method for Monotonic Equibiaxial Flexural Strength of Advanced Ceramics at Ambient Temperature. *Annu. Book ASTM Stand.* **2002**, Vol. 15.01.
12. ASTM C1499. Standard Test Method for Monotonic Equibiaxial Flexural Strength of Advanced Ceramics at Ambient Temperatures. *Annu. Book ASTM Stand.* **2001**, Vol. 15.01.
13. Vitman, F. F.; Pukh, V. P. A Method for Determining the Strength of Sheet Glass. *Aavodskaya Laboratoriya* **1963**, *29*, 863–67.

14. Determination of Bending Strength. Duetsches Institut fur Normung **1984**, *52*, 292.

15. ASTM C1239. Practice for Reporting Uniaxial Strength Data and Estimating Weibull Distribution Parameters for Advanced Ceramics. *Annu. Book ASTM Stand.* **2001**,Vol. 15.01.

16. AlliedSignal Engines. *Life Prediction Methodology for Ceramic Components of Advanced Heat Engines, Phase 1*. Phoenix, AZ, ORNL/Sub/89-SC674/1-2, DOE Office of Transportation Technologies, 1995.

17. ASTM C1322. Standard Practice for Fractography and Characterization of Fracture Origins in Advanced Ceramics. *Annu. Book ASTM Stand.* **2001**, Vol. 15.01.

18. Weil, N. A.; Daniel, I. M. Analysis of Failure Probabilities in Nonuniformly Stressed Brittle Materials. *Journal of the American Ceramic Society* **1964**, *47*, 268–74.

19. Batdorf, S. B. Some Approximate Treatments of Fracture Statistics for Polyaxial Tension. *International Journal of Fracture* **1977**, *13*, 5–11.

20. Breder, K.; Andersson, T.; Schölin, K. Fracture Strength of α- and β-SiAlON Measured by Biaxial and Four-Point Bending. *Journal of the American Ceramic Society* **1990**, *73*, 2128–30.

21. ASTM F417. Standard Test Method for Flexural Strength (Modulus of Rupture) of Electronic Grade Ceramics. *Annu. Book ASTM Stand.* **1998**, Vol. 10.04.

22. ASTM C1259. Standard Test Method for Dynamic Young's Modulus, Shear Modulus, and Poisson's Ratio for Advanced Ceramics by Impulse Excitation of Vibration. *Annu. Book ASTM Stand.* **2002**, Vol. 15.01.

23. ASTM E494. Standard Practice for Measuring Ultrasonic Velocity in Materials. *Annu. Book ASTM Stand.* **2000**, Vol. 3.03.

24. Rice, R. W.; Mecholsky, J. J., Jr.; Becher, P. F. The Effect of Grinding Direction on Flaw Character and Strength of Single Crystal and Polycrystalline Ceramics. *Journal of Materials Science* **1981**, *16*, 853–862.

25. Salem, J. A.; Nemeth, N. N.; Powers, L. M.; Choi, S. R. Reliability Analysis of Uniaxially Ground Brittle Materials. *Journal of Engineering for Gas Turbines and Power* **1996**, *118*, 863–71.

26. Wereszczak, A. A.; Kirkland, T. P.; Lin, H.-T.; Lee, S. K. Intermediate Temperature Inert Strength and Dynamic Fatigue of Candidate Silicon Nitrides for Diesel Exhaust Valves. *Ceramic Engineering and Science Proceedings* **2000**, *21*, 497–508.

27. Wereszczak, A. A.; Lin, H.-T.; Kirkland, T. P.; Andrews, M. J.; Lee, S. K. Strength and Dynamic Fatigue of Silicon Nitride at Intermediate Temperatures. In review, *Journal of Materials Science* **2001**.

28. Rice, R. W. Correlation of Machining-Grain-Size Effects on Tensile Strength with Tensile Strength-Grain-Size Behavior. *Journal of the American Ceramic Society* **1993**, *76*, 1068–70.

29. Rice, R. W. Effects of Ceramic Microstructural Character on Machining Direction – Strength Anisotropy. In *Machining of Advanced Materials, NIST Special Publication 847*; Jahanmir, S., Ed.; U.S. Department of Commerce **1993**, 185–204.

30. Wobker, H. G.; Tonshoff, H. K. High Efficiency Grinding of Structural Ceramics. In *Machining of Advanced Materials, NIST Special Publication 847*; Jahanmir, S., Ed.; U.S. Department of Commerce **1993**, *183*, 171–183.

31. Cho, S.-J.; Yoon, K.-J.; Kim, J.-J.; Kim, K.-H. Influence of Humidity on the Flexural Strength of Alumina, *Journal of the European Ceramic Society* **2000**, *20*, 761–764.

32. Cho, S.-J.; Yoon, K.-J.; Kim, J.-J.; Kim, K.-H. Effects of Environmental Temperature and Humidity on the Flexural Strength of Alumina and Measurement of Inert Strength, unpublished results.

33. Shockey, D. A.; Rowcliffe, D. J.; Dao, K. C.; Seaman, L. Particle Impact Damage in Silicon Nitride. *Journal of the American Ceramic Society* **1990**, *73*, 1613–19.

34. Sherman, D.; Brandon, D. G. The Ballistic Failure Mechanisms and Sequence in Semi-Infinite Supported Alumina Tiles. *Journal of Materials Research* **1997**, *12*, 1335–1343.

35. Sherman, D.; Ben-Shushan, T. Quasi-Static Impact Damage in Confined Ceramic Tiles. *International Journal of Impact Engineering* **1998**, *21*, 245–265.

36. Sherman, D. Impact Failure Mechanisms in Alumina Tiles on Finite Thickness Support and the Effect of Confinement. *International Journal of Impact Engineering* **2000**, *24*, 313–328.

37. Wereszczak, A. A.; Barnes, A. S.; Breder, K.; Binapal, S. Probabilistic Strength of {111} n-Type Silicon. *Journal of Materials Science: Materials in Electronics* **2000**, *11*, 291–303.

Appendix A. Failure Stress Values of All Uniaxial Flexure Specimens

As-Fired Chamfered	As-Received Chamfered	Longitudinal Chamfered	Transverse Chamfered	Rotational Chamfered	As-Fired Unchamfered	As-Received Unchamfered	Rotational Unchamfered
Uniaxial Flexure Failure Stress (MPa)	Uniaxial Flexure Failure Stress (MPa)	Uniaxial Flexure Failure Stress (MPa)	Uniaxial Flexure Failure Stress (MPa)	Uniaxial Flexure Failure Stress (MPa)	Uniaxial Flexure Failure Stress (MPa)	Uniaxial Flexure Failure Stress (MPa)	Uniaxial Flexure Failure Stress (MPa)
274.1	172.4	248.4	299.4	290.5	231.5	244.4	285.5
289.3	260.5	287.5	312.5	301.2	252.0	250.2	297.9
292.8	272.6	290.8	328.9	307.3	352.9	257.3	308.3
294.5	277.1	301.4	330.0	321.8	264.8	258.8	317.0
294.6	277.8	305.4	333.7	322.6	274.6	261.6	317.7
301.6	281.0	308.9	334.4	346.0	272.2	264.4	318.1
302.6	281.3	313.3	335.2	347.9	278.9	264.7	319.0
308.1	281.3	316.6	336.6	350.2	281.9	270.3	320.3
309.8	282.3	317.4	338.6	352.0	284.9	272.8	332.3
311.5	286.3	319.4	341.0	359.0	285.0	274.0	332.5
316.3	287.0	319.4	242.2	360.4	286.7	272.1	334.7
319.9	287.3	325.5	343.5	361.6	290.3	277.2	336.3
322.5	288.5	325.7	344.1	365.4	292.3	277.6	340.8
322.8	290.7	327.4	344.1	368.3	295.8	278.5	342.7
324.9	290.9	329.8	344.2	368.5	298.2	279.6	342.9
328.0	292.2	329.9	345.8	372.3	300.3	279.9	343.1
331.8	293.3	331.8	347.1	374.0	302.2	280.2	343.2
333.9	293.5	332.3	347.4	375.3	304.3	280.7	343.7
334.0	294.0	334.8	347.6	377.4	312.2	282.3	344.0
334.6	295.6	336.0	347.9	377.9	314.6	282.6	345.0
335.5	296.0	336.4	348.5	381.7	315.4	284.1	346.3
338.3	298.9	337.7	349.9	382.1	315.7	284.7	348.7
341.3	300.9	338.3	351.5	383.1	319.8	287.3	349.1
344.0	302.0	341.3	352.1	385.2	320.4	287.6	354.3
345.0	303.0	344.9	356.0	388.3	322.4	288.3	355.0
346.5	303.9	346.4	357.0	391.2	327.4	289.2	359.6
349.1	304.3	353.3	357.8	392.7	329.5	291.7	361.4
354.2	304.4	353.	365.6	—	333.4	292.9	—
357.9	305.6	—	—	—	340.2	294.5	—
367.5	305.7	—	—	—	341.8	299.1	—

INTENTIONALLY LEFT BLANK.

Appendix B. Failure Stress Values of All Equibiaxial Flexure Specimens

As-Fired	As-Received	Transverse (or Long)	Rotational
Equibiaxial Failure Stress (MPa)	**Equibiaxial Failure Stress (MPa)**	**Equibiaxial Failure Stress (MPa)**	**Equibiaxial Failure Stress (MPa)**
231.7	227.7	252.1	248.3
233.8	237.9	265.9	260.6
241.4	240.0	268.5	261.2
246.8	243.1	277.4	282.6
251.5	246.6	287.9	287.6
252.6	251.1	289.0	293.6
260.0	—	—	—
260.1	—	—	—
262.4	—	—	—
272.6	—	—	—
273.0	—	—	—
275.9	—	—	—
280.2	—	—	—

NO. OF
COPIES ORGANIZATION

1 (PDF ONLY) DEFENSE TECHNICAL INFORMATION CTR
DTIC OCA
8725 JOHN J KINGMAN RD
STE 0944
FORT BELVOIR VA 22060-6218

1 US ARMY RSRCH DEV & ENGRG CMD
SYSTEMS OF SYSTEMS INTEGRATION
AMSRD SS T
6000 6TH ST STE 100
FORT BELVOIR VA 22060-5608

1 INST FOR ADVNCD TCHNLGY
THE UNIV OF TEXAS
AT AUSTIN
3925 W BRAKER LN
AUSTIN TX 78759-5316

1 DIRECTOR
US ARMY RESEARCH LAB
IMNE ALC IMS
2800 POWDER MILL RD
ADELPHI MD 20783-1197

3 DIRECTOR
US ARMY RESEARCH LAB
AMSRD ARL CI OK TL
2800 POWDER MILL RD
ADELPHI MD 20783-1197

3 DIRECTOR
US ARMY RESEARCH LAB
AMSRD ARL CS IS T
2800 POWDER MILL RD
ADELPHI MD 20783-1197

ABERDEEN PROVING GROUND

1 DIR USARL
AMSRD ARL CI OK TP (BLDG 4600)

NO. OF COPIES ORGANIZATION

1 DIRECTOR
US ARMY RESEARCH LAB
AMSRD ARL SE DE
R ATKINSON
2800 POWDER MILL RD
ADELPHI MD 20783-1197

5 DIRECTOR
US ARMY RESEARCH LAB
AMSRD ARL WM MB
A ABRAHAMIAN
M BERMAN
M CHOWDHURY
T LI
E SZYMANSKI
2800 POWDER MILL RD
ADELPHI MD 20783-1197

1 COMMANDER
US ARMY MATERIEL CMD
AMXMI INT
5001 EISENHOWER AVE
ALEXANDRIA VA 22333-0001

2 PM MAS
SFAE AMO MAS MC
PICATINNY ARSENAL NJ
07806-5000

1 COMMANDER
US ARMY ARDEC
AMSTA AR CC
COL JENKER
PICATINNY ARSENAL NJ
07806-5000

1 COMMANDER
US ARMY ARDEC
AMSTA AR FSE
PICATINNY ARSENAL NJ
07806-5000

1 COMMANDER
US ARMY ARDEC
AMSTA AR TD
PICATINNY ARSENAL NJ
07806-5000

NO. OF COPIES ORGANIZATION

13 COMMANDER
US ARMY ARDEC
AMSTA AR CCH A
F ALTAMURA
M NICOLICH
M PALATHINGUL
D VO
R HOWELL
A VELLA
M YOUNG
L MANOLE
S MUSALLI
R CARR
M LUCIANO
E LOGSDEN
T LOUZEIRO
PICATINNY ARSENAL NJ
07806-5000

1 COMMANDER
US ARMY ARDEC
AMSTA AR CCH P
J LUTZ
PICATINNY ARSENAL NJ
07806-5000

1 COMMANDER
US ARMY ARDEC
AMSTA AR FSF T
C LIVECCHIA
PICATINNY ARSENAL NJ
07806-5000

1 COMMANDER
US ARMY ARDEC
AMSTA ASF
PICATINNY ARSENAL NJ
07806-5000

1 COMMANDER
US ARMY ARDEC
AMSTA AR QAC T C
J PAGE
PICATINNY ARSENAL NJ
07806-5000

1 COMMANDER
US ARMY ARDEC
AMSTA AR M
D DEMELLA
PICATINNY ARSENAL NJ
07806-5000

NO. OF COPIES ORGANIZATION

3 COMMANDER
US ARMY ARDEC
AMSTA AR FSA
A WARNASH
B MACHAK
M CHIEFA
PICATINNY ARSENAL NJ
07806-5000

2 COMMANDER
US ARMY ARDEC
AMSTA AR FSP G
M SCHIKSNIS
D CARLUCCI
PICATINNY ARSENAL NJ
07806-5000

2 COMMANDER
US ARMY ARDEC
AMSTA AR CCH C
H CHANIN
S CHICO
PICATINNY ARSENAL NJ
07806-5000

1 COMMANDER
US ARMY ARDEC
AMSTA AR QAC T
D RIGOGLIOSO
PICATINNY ARSENAL NJ
07806-5000

1 US ARMY ARDEC
INTELLIGENCE SPECIALIST
AMSTA AR WEL F
M GUERRIERE
PICATINNY ARSENAL NJ
07806-5000

9 COMMANDER
US ARMY ARDEC
AMSTA AR CCH B
P DONADIA
F DONLON
P VALENTI
C KNUTSON
G EUSTICE
K HENRY
J MCNABOC
R SAYER
F CHANG
PICATINNY ARSENAL NJ
07806-5000

NO. OF COPIES ORGANIZATION

1 PM ARMS
SFAE GCSS ARMS
BLDG 171
PICATINNY ARSENAL NJ
07806-5000

1 COMMANDER
US ARMY ARDEC
AMSTA AR WEA
J BRESCIA
PICATINNY ARSENAL NJ
07806-5000

1 PM MAS
SFAE AMO MAS
PICATINNY ARSENAL NJ
07806-5000

1 PM MAS
SFAE AMO MAS
CHIEF ENGINEER
PICATINNY ARSENAL NJ
07806-5000

1 PM MAS
SFAE AMO MAS PS
PICATINNY ARSENAL NJ
07806-5000

2 PM MAS
SFAE AMO MAS LC
PICATINNY ARSENAL NJ
07806-5000

1 COMMANDER
US ARMY TACOM
PM COMBAT SYSTEMS
SFAE GCS CS
6501 ELEVEN MILE RD
WARREN MI 48397-5000

1 COMMANDER
US ARMY TACOM
AMSTA SF
WARREN MI 48397-5000

1 DIRECTOR
AIR FORCE RESEARCH LAB
MLLMD
D MIRACLE
2230 TENTH ST
WRIGHT PATTERSON AFB OH
45433-7817

NO. OF COPIES ORGANIZATION

1 OFC OF NAVAL RESEARCH
J CHRISTODOULOU
ONR CODE 332
800 N QUINCY ST
ARLINGTON VA 22217-5600

1 COMMANDER
US ARMY TACOM
PM SURVIVABLE SYSTEMS
SFAE GCSS W GSI H
M RYZYI
6501 ELEVEN MILE RD
WARREN MI 48397-5000

1 COMMANDER
US ARMY TACOM
CHIEF ABRAMS TESTING
SFAE GCSS W AB QT
T KRASKIEWICZ
6501 ELEVEN MILE RD
WARREN MI 48397-5000

1 COMMANDER
WATERVLIET ARSENAL
SMCWV QAE Q
B VANINA
BLDG 44
WATERVLIET NY 12189-4050

2 HQ IOC TANK
AMMUNITION TEAM
AMSIO SMT
R CRAWFORD
W HARRIS
ROCK ISLAND IL 61299-6000

2 COMMANDER
US ARMY AMCOM
AVIATION APPLIED TECH DIR
J SCHUCK
FORT EUSTIS VA 23604-5577

1 NSWC
DAHLGREN DIV CODE G06
DAHLGREN VA 22448

2 US ARMY CORPS OF ENGR
CERD C
T LIU
CEW ET
T TAN
20 MASSACHUSETTS AVE NW
WASHINGTON DC 20314

NO. OF COPIES ORGANIZATION

1 US ARMY COLD REGIONS
RSCH & ENGRNG LAB
P DUTTA
72 LYME RD
HANOVER NH 03755

13 COMMANDER
US ARMY TACOM
AMSTA TR R
R MCCLELLAND
D THOMAS
J BENNETT
D HANSEN
AMSTA JSK
S GOODMAN
J FLORENCE
D TEMPLETON
A SCHUMACHER
AMSTA TR D
D OSTBERG
L HINOJOSA
B RAJU
AMSTA CS SF
H HUTCHINSON
F SCHWARZ
WARREN MI 48397-5000

14 BENET LABS
AMSTA AR CCB
R FISCELLA
M SOJA
E KATHE
M SCAVULO
G SPENCER
P WHEELER
S KRUPSKI
J VASILAKIS
G FRIAR
R HASENBEIN
AMSTA CCB R
S SOPOK
E HYLAND
D CRAYON
R DILLON
WATERVLIET NY 12189-4050

1 USA SBCCOM PM SOLDIER SPT
AMSSB PM RSS A
J CONNORS
KANSAS ST
NATICK MA 01760-5057

NO. OF COPIES ORGANIZATION

1 NSWC
TECH LIBRARY CODE B60
17320 DAHLGREN RD
DAHLGREN VA 22448

2 USA SBCCOM
MATERIAL SCIENCE TEAM
AMSSB RSS
J HERBERT
M SENNETT
KANSAS ST
NATICK MA 01760-5057

2 OFC OF NAVAL RESEARCH
D SIEGEL CODE 351
J KELLY
800 N QUINCY ST
ARLINGTON VA 22217-5660

1 NSWC
CRANE DIVISION
M JOHNSON CODE 20H4
LOUISVILLE KY 40214-5245

2 NSWC
U SORATHIA
C WILLIAMS CODE 6551
9500 MACARTHUR BLVD
WEST BETHESDA MD 20817

2 COMMANDER
NSWC
CARDEROCK DIVISION
R PETERSON CODE 2020
M CRITCHFIELD CODE 1730
BETHESDA MD 20084

8 DIRECTOR
US ARMY NGIC
D LEITER MS 404
M HOLTUS MS 301
M WOLFE MS 307
S MINGLEDORF MS 504
J GASTON MS 301
W GSTATTENBAUER MS 304
R WARNER MS 305
J CRIDER MS 306
2055 BOULDERS RD
CHARLOTTESVILLE VA
22911-8318

NO. OF COPIES ORGANIZATION

1 NAVAL SEA SYSTEMS CMD
D LIESE
1333 ISAAC HULL AVE SE 1100
WASHINGTON DC 20376-1100

7 US ARMY SBCCOM
SOLDIER SYSTEMS CENTER
BALLISTICS TEAM
J WARD
W ZUKAS
P CUNNIFF
J SONG
MARINE CORPS TEAM
J MACKIEWICZ
AMSSB RCP SS
W NYKVIST
S BEAUDOIN
KANSAS ST
NATICK MA 01760-5019

7 US ARMY RESEARCH OFC
A CROWSON
H EVERITT
J PRATER
G ANDERSON
D STEPP
D KISEROW
J CHANG
PO BOX 12211
RESEARCH TRIANGLE PARK NC
27709-2211

1 AFRL MLBC
2941 P ST RM 136
WRIGHT PATTERSON AFB OH
45433-7750

1 DIRECTOR
LOS ALAMOS NATL LAB
F L ADDESSIO T 3 MS 5000
PO BOX 1633
LOS ALAMOS NM 87545

8 NSWC
J FRANCIS CODE G30
D WILSON CODE G32
R D COOPER CODE G32
J FRAYSSE CODE G33
E ROWE CODE G33
T DURAN CODE G33
L DE SIMONE CODE G33
R HUBBARD CODE G33
DAHLGREN VA 22448

NO. OF COPIES ORGANIZATION

1 NSWC
CARDEROCK DIVISION
R CRANE CODE 6553
9500 MACARTHUR BLVD
WEST BETHESDA MD 20817-5700

1 AFRL MLMP
R THOMSON
2977 HOBSON WAY
BLDG 653 RM 215
WRIGHT PATTERSON AFB OH
45433-7739

2 AFRL MLMP
F ABRAMS
J BROWN
2977 HOBSON WAY
BLDG 653 RM 215
WRIGHT PATTERSON AFB OH
45433-7739

5 DIRECTOR
LLNL
R CHRISTENSEN
S DETERESA
F MAGNESS
M FINGER MS 313
M MURPHY L 282
PO BOX 808
LIVERMORE CA 94550

1 AFRL MLS OL
L COULTER
5851 F AVE
BLDG 849 RM AD1A
HILL AFB UT 84056-5713

1 OSD
JOINT CCD TEST FORCE
OSD JCCD
R WILLIAMS
3909 HALLS FERRY RD
VICKSBURG MS 29180-6199

3 DARPA
M VANFOSSEN
S WAX
L CHRISTODOULOU
3701 N FAIRFAX DR
ARLINGTON VA 22203-1714

NO. OF COPIES ORGANIZATION

1 OAK RIDGE NATL LAB
R M DAVIS
PO BOX 2008
OAK RIDGE TN 37831-6195

1 OAK RIDGE NATL LAB
C EBERLE MS 8048
PO BOX 2008
OAK RIDGE TN 37831

3 DIRECTOR
SANDIA NATL LABS
APPLIED MECHS DEPT
MS 9042
J HANDROCK
Y R KAN
J LAUFFER
PO BOX 969
LIVERMORE CA 94551-0969

1 OAK RIDGE NATL LAB
C D WARREN MS 8039
PO BOX 2008
OAK RIDGE TN 37831

4 NIST
M VANLANDINGHAM MS 8621
J CHIN MS 8621
J MARTIN MS 8621
D DUTHINH MS 8611
100 BUREAU DR
GAITHERSBURG MD 20899

1 HYDROGEOLOGIC INC
SERDP ESTCP SPT OFC
S WALSH
1155 HERNDON PKWY STE 900
HERNDON VA 20170

3 NASA LANGLEY RESEARCH CTR
AMSRD ARL VT
W ELBER MS 266
F BARTLETT JR MS 266
G FARLEY MS 266
HAMPTON VA 23681-0001

1 FHWA
E MUNLEY
6300 GEORGETOWN PIKE
MCLEAN VA 22101

NO. OF COPIES ORGANIZATION

1 USDOT FEDERAL RAILROAD
M FATEH RDV 31
WASHINGTON DC 20590

3 CYTEC FIBERITE
R DUNNE
D KOHLI
R MAYHEW
1300 REVOLUTION ST
HAVRE DE GRACE MD 21078

1 DIRECTOR
NGIC
IANG TMT
2055 BOULDERS RD
CHARLOTTESVILLE VA
22911-8318

2 3TEX CORP
A BOGDANOVICH
J SINGLETARY
109 MACKENAN DR
CARY NC 27511

1 DIRECTOR
DEFENSE INTLLGNC AGNCY
TA 5
K CRELLING
WASHINGTON DC 20310

1 COMPOSITE MATERIALS INC
D SHORTT
19105 63 AVE NE
PO BOX 25
ARLINGTON WA 98223

1 JPS GLASS
L CARTER
PO BOX 260
SLATER RD
SLATER SC 29683

1 COMPOSITE MATERIALS INC
R HOLLAND
11 JEWEL CT
ORINDA CA 94563

1 COMPOSITE MATERIALS INC
C RILEY
14530 S ANSON AVE
SANTA FE SPRINGS CA 90670

NO. OF COPIES ORGANIZATION

1 SIMULA
R HUYETT
10016 S 51ST ST
PHOENIX AZ 85044

2 PROTECTION MATERIALS INC
M MILLER
F CRILLEY
14000 NW 58 CT
MIAMI LAKES FL 33014

2 FOSTER MILLER
M ROYLANCE
W ZUKAS
195 BEAR HILL RD
WALTHAM MA 02354-1196

1 ROM DEVELOPMENT CORP
R O MEARA
136 SWINEBURNE ROW
BRICK MARKET PLACE
NEWPORT RI 02840

2 TEXTRON SYSTEMS
M TREASURE
T FOLTZ
1449 MIDDLESEX ST
LOWELL MA 01851

1 O GARA HESS & EISENHARDT
M GILLESPIE
9113 LESAINT DR
FAIRFIELD OH 45014

1 MILLIKEN RESEARCH CORP
M MACLEOD
PO BOX 1926
SPARTANBURG SC 29303

1 CONNEAUGHT INDUSTRIES INC
J SANTOS
PO BOX 1425
COVENTRY RI 02816

1 ARMTEC DEFENSE PRODUCTS
S DYER
85 901 AVE 53
PO BOX 848
COACHELLA CA 92236

NO. OF COPIES ORGANIZATION

3 PACIFIC NORTHWEST LAB
M SMITH
G VAN ARSDALE
R SHIPPELL
PO BOX 999
RICHLAND WA 99352

1 ALLIANT TECHSYSTEMS INC
4700 NATHAN LN N
PLYMOUTH MN 55442-2512

1 APPLIED COMPOSITES
W GRISCH
333 NORTH SIXTH ST
ST CHARLES IL 60174

1 CUSTOM ANALYTICAL
ENG SYS INC
A ALEXANDER
13000 TENSOR LANE NE
FLINTSTONE MD 21530

1 AAI CORP
DR N B MCNELLIS
PO BOX 126
HUNT VALLEY MD 21030-0126

1 OFC DEPUTY UNDER SEC DEFNS
J THOMPSON
1745 JEFFERSON DAVIS HWY
CRYSTAL SQ 4 STE 501
ARLINGTON VA 22202

3 ALLIANT TECHSYSTEMS INC
J CONDON
E LYNAM
J GERHARD
WV01 16 STATE RT 956
PO BOX 210
ROCKET CENTER WV
26726-0210

1 PROJECTILE TECHNOLOGY INC
515 GILES ST
HAVRE DE GRACE MD 21078

1 PRATT & WHITNEY
C WATSON
400 MAIN ST MS 114 37
EAST HARTFORD CT 06108

NO. OF COPIES ORGANIZATION

5 NORTHROP GRUMMAN
B IRWIN
K EVANS
D EWART
A SHREKENHAMER
J MCGLYNN
BLDG 160 DEPT 3700
1100 W HOLLYVALE ST
AZUSA CA 91701

1 BRIGS COMPANY
J BACKOFEN
2668 PETERBOROUGH ST
HERNDON VA 22071-2443

1 ZERNOW TECHNICAL SERVICES
L ZERNOW
425 W BONITA AVE STE 208
SAN DIMAS CA 91773

2 GENERAL DYNAMICS OTS
FLINCHBAUGH DIV
K LINDE
T LYNCH
PO BOX 127
RED LION PA 17356

1 GKN WESTLAND AEROSPACE
D OLDS
450 MURDOCK AVE
MERIDEN CT 06450-8324

5 SIKORSKY AIRCRAFT
G JACARUSO
T CARSTENSAN
B KAY
S GARBO MS S330A
J ADELMANN
6900 MAIN ST
PO BOX 9729
STRATFORD CT 06497-9729

1 AEROSPACE CORP
G HAWKINS M4 945
2350 E EL SEGUNDO BLVD
EL SEGUNDO CA 90245

2 CYTEC FIBERITE
M LIN
W WEB
1440 N KRAEMER BLVD
ANAHEIM CA 92806

NO. OF COPIES	ORGANIZATION
2	UDLP G THOMAS M MACLEAN PO BOX 58123 SANTA CLARA CA 95052
2	UDLP R BRYNSVOLD P JANKE MS 170 4800 E RIVER RD MINNEAPOLIS MN 55421-1498
1	LOCKHEED MARTIN SKUNK WORKS D FORTNEY 1011 LOCKHEED WAY PALMDALE CA 93599-2502
1	NORTHRUP GRUMMAN CORP ELECTRONIC SENSORS & SYSTEMS DIV E SCHOCH MS V 16 1745A W NURSERY RD LINTHICUM MD 21090
1	GDLS DIVISION D BARTLE PO BOX 1901 WARREN MI 48090
2	GDLS D REES M PASIK PO BOX 2074 WARREN MI 48090-2074
1	GDLS MUSKEGON OPER M SOIMAR 76 GETTY ST MUSKEGON MI 49442
1	GENERAL DYNAMICS AMPHIBIOUS SYS SURVIVABILITY LEAD G WALKER 991 ANNAPOLIS WAY WOODBRIDGE VA 22191
6	INST FOR ADVANCED TECH H FAIR I MCNAB P SULLIVAN S BLESS W REINECKE C PERSAD 3925 W BRAKER LN STE 400 AUSTIN TX 78759-5316
1	ARROW TECH ASSOC 1233 SHELBURNE RD STE D8 SOUTH BURLINGTON VT 05403-7700
1	R EICHELBERGER CONSULTANT 409 W CATHERINE ST BEL AIR MD 21014-3613
1	SAIC G CHRYSSOMALLIS 8500 NORMANDALE LAKE BLVD SUITE 1610 BLOOMINGTON MN 55437-3828
1	UCLA MANE DEPT ENGR IV H T HAHN LOS ANGELES CA 90024-1597
1	UMASS LOWELL PLASTICS DEPT N SCHOTT 1 UNIVERSITY AVE LOWELL MA 01854
1	IIT RESEARCH CTR D ROSE 201 MILL ST ROME NY 13440-6916
1	GA TECH RESEARCH INST GA INST OF TCHNLGY P FRIEDERICH ATLANTA GA 30392
1	MICHIGAN ST UNIV MSM DEPT R AVERILL 3515 EB EAST LANSING MI 48824-1226

NO. OF COPIES ORGANIZATION

1 PENN STATE UNIV
R S ENGEL
245 HAMMOND BLDG
UNIVERSITY PARK PA 16801

1 PENN STATE UNIV
C BAKIS
212 EARTH ENGR
SCIENCES BLDG
UNIVERSITY PARK PA 16802

1 PURDUE UNIV
SCHOOL OF AERO & ASTRO
C T SUN
W LAFAYETTE IN 47907-1282

1 UNIV OF MAINE
ADV STR & COMP LAB
R LOPEZ ANIDO
5793 AEWC BLDG
ORONO ME 04469-5793

1 JOHNS HOPKINS UNIV
APPLIED PHYSICS LAB
P WIENHOLD
11100 JOHNS HOPKINS RD
LAUREL MD 20723-6099

1 UNIV OF DAYTON
J M WHITNEY
COLLEGE PARK AVE
DAYTON OH 45469-0240

5 UNIV OF DELAWARE
CTR FOR COMPOSITE MTRLS
J GILLESPIE
M SANTARE
S YARLAGADDA
S ADVANI
D HEIDER
201 SPENCER LAB
NEWARK DE 19716

1 DEPT OF MTRLS
SCIENCE & ENGRG
UNIV OF ILLINOIS
AT URBANA CHAMPAIGN
J ECONOMY
1304 W GREEN ST 115B
URBANA IL 61801

NO. OF COPIES ORGANIZATION

1 MISSISSIPPI STATE UNIV
DEPT OF AEROSPACE ENGRG
A J VIZZINI
MISSISSIPPI STATE MS 39762

1 DREXEL UNIV
A S D WANG
3141 CHESTNUT ST
PHILADELPHIA PA 19104

3 UNIV OF TEXAS AT AUSTIN
CTR FOR ELECTROMECHANICS
J PRICE
A WALLS
J KITZMILLER
10100 BURNET RD
AUSTIN TX 78758-4497

1 SOUTHWEST RESEARCH INST
ENGR & MATL SCIENCES DIV
J RIEGEL
6220 CULEBRA RD
PO DRAWER 28510
SAN ANTONIO TX 78228-0510

3 DIRECTOR
US ARMY RESEARCH LAB
AMSRD ARL WM MB
A FRYDMAN
2800 POWDER MILL RD
ADELPHI MD 20783-1197

ABERDEEN PROVING GROUND

1 US ARMY ATC
CSTE DTC AT AC I
W C FRAZER
400 COLLERAN RD
APG MD 21005-5059

88 DIR USARL
AMSRD ARL CI
AMSRD ARL O AP EG
M ADAMSON
AMSRD ARL SL BA
AMSRD ARL SL BB
D BELY
AMSRD ARL WM
J SMITH
AMSRD ARL WM B
CHIEF
T KOGLER
AMSRD ARL WM BA
D LYON

NO. OF
COPIES ORGANIZATION

AMSRD ARL WM BC
J NEWILL
P PLOSTINS
AMSRD ARL WM BD
P CONROY
B FORCH
M LEADORE
C LEVERITT
R LIEB
R PESCE-RODRIGUEZ
B RICE
A ZIELINSKI
AMSRD ARL WM BF
S WILKERSON
AMSRD ARL WM M
J MCCAULEY
S MCKNIGHT
AMSRD ARL WM MA
CHIEF
L GHIORSE
E WETZEL
AMSRD ARL WM MB
J BENDER
T BOGETTI
J BROWN
L BURTON
R CARTER
K CHO
W DE ROSSET
G DEWING
R DOWDING
W DRYSDALE
R EMERSON
D GRAY
D HOPKINS
R KASTE
L KECSKES
M MINNICINO
B POWERS
D SNOHA
J SOUTH
M STAKER
J SWAB
J TZENG
AMSRD ARL WM MC
CHIEF
R BOSSOLI
E CHIN
S CORNELISON
D GRANVILLE
B HART
J LASALVIA
J MONTGOMERY
F PIERCE

NO. OF
COPIES ORGANIZATION

E RIGAS
W SPURGEON
AMSRD ARL WM MD
B CHEESEMAN
P DEHMER
R DOOLEY
G GAZONAS
S GHIORSE
M KLUSEWITZ
W ROY
J SANDS
D SPAGNUOLO
S WALSH
S WOLF
AMSRD ARL WM RP
J BORNSTEIN
C SHOEMAKER
AMSRD ARL WM T
B BURNS
AMSRD ARL WM TA
W BRUCHEY
M BURKINS
W GILLICH
B GOOCH
T HAVEL
C HOPPEL
E HORWATH
J RUNYEON
M ZOLTOSKI
AMSRD ARL WM TB
P BAKER
AMSRD ARL WM TC
R COATES
AMSRD ARL WM TD
D DANDEKAR
M RAFTENBERG
S SCHOENFELD
T WEERASOORIYA
AMSRD ARL WM TE
CHIEF
J POWELL

NO. OF COPIES ORGANIZATION

1 LTD
R MARTIN
MERL
TAMWORTH RD
HERTFORD SG13 7DG
UK

1 CIVIL AVIATION
ADMINSTRATION
T GOTTESMAN
PO BOX 8
BEN GURION INTRNL AIRPORT
LOD 70150
ISRAEL

1 AEROSPATIALE
S ANDRE
A BTE CC RTE MD132
316 ROUTE DE BAYONNE
TOULOUSE 31060
FRANCE

1 DRA FORT HALSTEAD
P N JONES
SEVEN OAKS KENT TN 147BP
UK

1 SWISS FEDERAL ARMAMENTS
WKS
W LANZ
ALLMENDSTRASSE 86
3602 THUN
SWITZERLAND

1 DYNAMEC RESEARCH LAB
AKE PERSSON
BOX 201
SE 151 23 SODERTALJE
SWEDEN

1 ISRAEL INST OF TECHLGY
S BODNER
FACULTY OF MECHANICAL
ENGR
HAIFA 3200
ISRAEL

1 DSTO
WEAPONS SYSTEMS DIVISION
N BURMAN RLLWS
SALISBURY
SOUTH AUSTRALIA 5108
AUSTRALIA

NO. OF COPIES ORGANIZATION

1 DEF RES ESTABLISHMENT
VALCARTIER
A DUPUIS
2459 BLVD PIE XI NORTH
VALCARTIER QUEBEC
CANADA
PO BOX 8800 COURCELETTE
GOA IRO QUEBEC
CANADA

1 ECOLE POLYTECH
J MANSON
DMX LTC
CH 1015 LAUSANNE
SWITZERLAND

1 TNO DEFENSE SECURITY & SAFETY
R R IJSSELSTEIN
PO BOX 96864
2509 JG THE HAGUE
THE NETHERLANDS

2 FOA NATL DEFENSE RESEARCH
ESTAB
DIR DEPT OF WEAPONS &
PROTECTION
B JANZON
R HOLMLIN
S 172 90 STOCKHOLM
SWEDEN

2 DEFENSE TECH & PROC
AGENCY GROUND
I CREWTHER
GENERAL HERZOG HAUS
3602 THUN
SWITZERLAND

1 MINISTRY OF DEFENCE
RAFAEL
ARMAMENT DEVELOPMENT
AUTH
M MAYSELESS
PO BOX 2250
HAIFA 31021
ISRAEL

1 B HIRSCH
TACHKEMONY ST 6
NETAMUA 42611
ISRAEL

NO. OF COPIES	ORGANIZATION
1	DEUTSCHE AEROSPACE AG DYNAMICS SYSTEMS M HELD PO BOX 1340 D 86523 SCHROBENHAUSEN GERMANY

NO. OF COPIES ORGANIZATION

1 DARPA
SPECIAL PROJECTS OFFICE
J CARLINI
3701 N FAIRFAX DR
ARLINGTON VA 22203-1714

2 CERADYNE
J SHIH
B MIKIJELK
3169 REDHILL AVE
COSTA MESA CA 92626

2 CERCOM
D ASHKIN
R PALICKA
1960 WATSON WAY
VISTA CA 92083

2 COMMANDER
US ARMY TACOM
AMSTA JSK
L FRANKS
D TEMPLETON
WARREN MI 48397-5000

1 CONNECTICUT RESERVE TECH
S DUFFY
2400 SUPERIOR AVE #208
CLEVELAND OH 44114

1 COORSTEK
B SEEGMILLER
600 9TH ST
GOLDEN CO 80401

1 NATIONAL INST OF STDS & TECH
G QUINN
BLDG 223 RM A256
100 BUREAU DRIVE STOP 8520
GAITHERSBURG MD 20899-8520

1 NASA GRC
J SALEM
MS-49-7
21000 BROOKPARK RD
CLEVELAND OH 44135

1 NETWORK COMPUTING SERVICES
T HOLMQUIST
1200 WASHINGTON AVE S
MINNEAPOLIS MN 55415

NO. OF COPIES ORGANIZATION

10 OAK RIDGE NATIONAL LAB
A WERESZCZAK
PO BOX 2008
BLDG 4515 MS 6068
OAK RIDGE TN 37831-6068

4 RUTGERS STATE UNIV OF NJ
R CANNON
V GREENHUT
R HABER
D NIESZ
CENTER FOR CERAMIC RSCH
607 TAYLOR RD
PISCATAWAY NJ 08854-8065

1 SAINT GOBAIN ABRASIVES
K BREDER
HIGGINS GRINDING TECH CTR
1 NEW BOND ST MS 413-201
WORCESTER MA 01615-0008

1 SAINT GOBAIN/CARBORUNDUM
J RUPPEL
23 ACHESON DR
NIAGARA FALLS NY 14303

2 SAINT GOBAIN IND CERAMICS
R LICHT
V PUJARI
1 GODDARD RD
NORTHBORO MA 01532-1545

1 UNIV OF DAYTON RSCH INST
R WILLS
CERAMIC AND GLASS LABS
300 COLLEGE PARK
DAYTON OH 45469-0182

4 US ARMY RESEARCH OFC
B LAMATTINA
W MULLINS
A RAJENDRA
E SEGAN
PO BOX 12211
RESEARCH TRIANGLE PARK NC
27709-2211

NO. OF
COPIES ORGANIZATION

1 USA SBCCOM
SOLDIER SYSTEMS CENTER
AMSSB RCP SS
KANSAS ST
NATICK MA 01760-5019

1 M CUBED TECHNOLOGIES
M AGHAJANIAN
1 TRALEE INDUSTRIAL PARK
NEWARK DE 19711

1 MER CORP
LORI BRACAMONTE
7960 KOLB ROAD
TUCSON AZ 85706

2 MINE SAFETY APPLIANCES CO
T MOYNIHAN
C HORT
1100 CRANBERRY WOODS DRIVE
CRANBERRY TWP PA 16066

1 SUPERIOR GRAPHITE
D LAUGHTON
1807 SHORELINE DRIVE
ST CHARLES IL 60174

1 SIMULA
D MARCHANT
7822 SOUTH 46TH STREET
PHOENIX AZ 85044

ABERDEEN PROVING GROUND

9 DIR USARL
AMSRD ARL WM MA
M VANLANDINGHAM
AMSRD ARL WM MC
M MAHER
AMSRD ARL WM MD
J ADAMS
K TACKITT
B SCOTT
P HUANG
K DOHERTY
J CAMPBELL
AMSRD ARL WM TD
N RUPERT